Rock Mechanics and Rock Engineering (2024) 57:1195–1217
https://doi.org/10.1007/s00603-023-03607-6

ORIGINAL PAPER

Probability-Based Design of Reinforced Rock Slopes Using Coupled FORM and Monte Carlo Methods

Bak Kong Low[1,2] · **Chia Weng Boon**[3]

Received: 31 May 2023 / Accepted: 4 October 2023 / Published online: 6 November 2023
© The Author(s) 2023

Abstract

The efficiency of the first-order reliability method (FORM) and the accuracy of Monte Carlo simulations (MCS) are coupled in probability-based designs of reinforced rock slopes, including a Hong Kong slope with exfoliation joints. Load–resistance duality is demonstrated and resolved automatically in a foundation on rock with a discontinuity plane. Other examples include the lengthy Hoek and Bray deterministic vectorial procedure for comprehensive pentahedral blocks with external load and bolt force, which is made efficient and more succinct before extending it to probability-based design via MCS-enhanced FORM. The FORM–MCS–FORM design procedure is proposed for cases with multiple failure modes. For cases with a dominant single failure mode, the time-saving importance sampling (IS) and the fast second-order reliability method (SORM) can be used in lieu of MCS. Two cases of 3D reinforced blocks (pentahedral and tetrahedral, respectively) with the possibility of multiple sliding modes are investigated. In the case of the reinforced pentahedral block, direct MCS shows that there is only one dominant failure mode, for which the efficient method of importance sampling at the FORM design point provides fast verification of the revised design. In the case of the reinforced tetrahedral block, there are multiple failure modes contributing to the total failure probability, for which the proposed MCS-enhanced FORM procedure is demonstrated to be essential. Comparisons are made between Excel MCS and MATLAB MCS.

Highlights

- Probability-based design of a Hong Kong slope via coupled FORM and Monte Carlo methods.
- Efficient analysis of a bolted pentahedral block based on Hoek-Bray procedure and Excel Solver.
- New extension of Low-and-Tang FORM algorithm to MCS involving correlated nonnormals.
- FORM-MCS-FORM method for design of 3D rock slopes with multiple failure domains.
- Importance sampling or SORM in lieu of MCS for cases with a dominant single failure mode.

Keywords Rock slopes · Pentahedral · Tetrahedral · Probability · Monte Carlo · Importance sampling · FORM · SORM

1 Introduction

The probability of failure (P_f) estimated from the FORM reliability index β using the following equation is *approximate* when the random variables are nonnormally distributed and/or the limit state surface (LSS) is curved:

$$FORM \quad P_f \approx 1 - \Phi(\beta) = \Phi(-\beta). \tag{1}$$

In reliability-based design (RBD), it is desirable to determine P_f more accurately, by (i) direct Monte Carlo simulation (direct MCS), or (ii) importance sampling (IS) around

✉ Bak Kong Low
bklow@alum.mit.edu

Chia Weng Boon
chiaweng.boon@oxfordalumni.org

[1] Nanyang Technological University, Singapore, Singapore

[2] Present Address: Research Affiliate, MIT, Cambridge, MA, USA

[3] Gamuda Engineering Sdn Bhd, 47820 Petaling Jaya, Selangor, Malaysia

the design point located by FORM, or (iii) the second-order reliability method (SORM) which estimates component curvatures at the FORM design point. It is demonstrated in this study that the more accurate methods of determining P_f by direct MCS, IS and SORM can be easily implemented as extensions of the Low and Tang (2007) Excel FORM template, such that FORM provides the basis for IS and SORM, which in turn provide a near-exact probability of failure for a revised design by FORM. It will be appreciated from the probability-based design examples in this study that the word *coupled* in the paper's title implies "*mutually advantageous*" for FORM and MCS. Note that importance sampling is a Monte Carlo method, which is less time-consuming than direct MCS. The FORM–MCS–FORM design procedure presented in this study is more accurate and efficient than using either FORM or MCS alone.

A quick grasp of the efficient Excel FORM method is presented next.

1.1 Overview of the Low and Tang (2007) FORM Method Prior to Coupled FORM–MCS

The FORM extends the Hasofer–Lind (1974) index (for correlated *normal* variates) to deal with correlated *non-normal* random variates, and hence includes the earlier Hasofer–Lind index as a special case. The classical intricate FORM procedure in the rotated **u** space is mathematically elegant, as explained (or discussed) in commendable details in Ditlevsen (1981), Shinozuka (1983), Ang and Tang (1984), Der Kiureghian and Liu (1986), Madsen et al. (1986), Melchers (1987), Tichy (1993), Haldar and Mahadevan (2000), Rackwitz (2001), Baecher and Christian (2003), Kottegoda and Rosso (2008), and Melchers and Beck (2018), for example.

This study on the probability-based design of rock slopes uses the more intuitive and efficient Low and Tang (2007) spreadsheet-automated algorithm, which obtains the same solutions as the mathematically intricate classical FORM procedure.

In FORM, the reliability index β can be written as follows:

$$\beta = \min_{\mathbf{x}\in F} \sqrt{\left[\frac{x_i - \mu_i^N}{\sigma_i^N}\right]^T \mathbf{R}^{-1} \left[\frac{x_i - \mu_i^N}{\sigma_i^N}\right]}, \tag{2a}$$

where **R** is the correlation matrix, and μ_i^N and σ_i^N are *equivalent normal* mean and *equivalent normal* standard deviation values, which can be calculated by the Rackwitz–Fiessler (1978) transformation:

$$\text{Equivalent normal standard deviation}: \ \sigma^N = \frac{\phi\{\Phi^{-1}[F(x)]\}}{f(x)}, \tag{2b}$$

$$\text{Equivalent normal mean}: \ \mu^N = x - \sigma^N \times \Phi^{-1}[F(x)], \tag{2c}$$

where x is the original non-normal variate, $\Phi^{-1}[.]$ is the inverse of the cumulative probability (CDF) of a standard normal distribution, $F(x)$ is the original non-normal CDF evaluated at x, $\phi\{.\}$ is the probability density function (pdf) of the standard normal distribution, and $f(x)$ is the original non-normal probability density ordinates at x. Equation 2 was used in the Low and Tang (2004) Excel-automated FORM procedure. One can regard the computation of the FORM β by Eq. 2 as that of finding the smallest *equivalent* hyper-ellipsoid (centered at the *equivalent* normal mean-value point $\boldsymbol{\mu}^N$ and with *equivalent* normal standard deviations $\boldsymbol{\sigma}^N$) that is tangent to the LSS. Hence, for correlated non-normals, the ellipsoidal perspective still applies in the original coordinate system, except that the non-normal distributions are replaced by an equivalent normal ellipsoid.

An alternative FORM computational approach was given in Low and Tang (2007), summarized in Fig. 1, which uses the following equation for the reliability index β:

$$\beta = \min_{\mathbf{x}\in F} \sqrt{\mathbf{n}^T \mathbf{R}^{-1} \mathbf{n}} \ \text{(Obviating the calculations of } \mu_i^N \text{ and } \sigma_i^N\text{)} \tag{3}$$

where **n** is the dimensionless vector defined by the bracketed term in Eq. 2(a). The above equation can be entered easily as an Excel array formula using Excel matrix functions *mmult*, *transpose* and *minverse*. For each value of the vector **n** tried by the Excel Solver in the Low and Tang (2007) FORM method, a short Excel VBA function code x_i(DistributionName, para, ni), shown in Fig. 9 of the Appendix, automates the computation of x_i from n_i, for use in the constraint $g(\mathbf{x}) = 0$, via the following equation:

$$x_i = F^{-1}\left[\Phi\left(n_i\right)\right] \ \text{(inversed from } \ F\left(x_i\right) = \Phi\left(n_i\right)\text{)} \tag{4}$$

in which $F(x_i)$ is the original non-normal CDF of x_i, and $\Phi(n_i)$ is the standard normal CDF.

Figure 1 provides an illustration involving three correlated non-Gaussian variables, for which the performance function is $g(\mathbf{x}) = VW - Z$. Failure is reached when the resistances V and W decrease from their mean values to their most probable failure values of 33.12 and 40.12, and the load Z increases from its mean value to its most probable failure value of 1329. The most probable point (MPP) of failure (33.12, 40.12, 1329) is the point where the expanding 3D equivalent dispersion ellipsoid first touches the LSS. This MPP is a failure state because $33.12 \times 40.12 = 1329$. Much valuable information and insights are provided by the MPP of failure (the **x*** values) and the sensitivity indicators (the **n*** values), as discussed in Low (2021; 2022), and Low and Bathurst (2022). The focus in this paper is

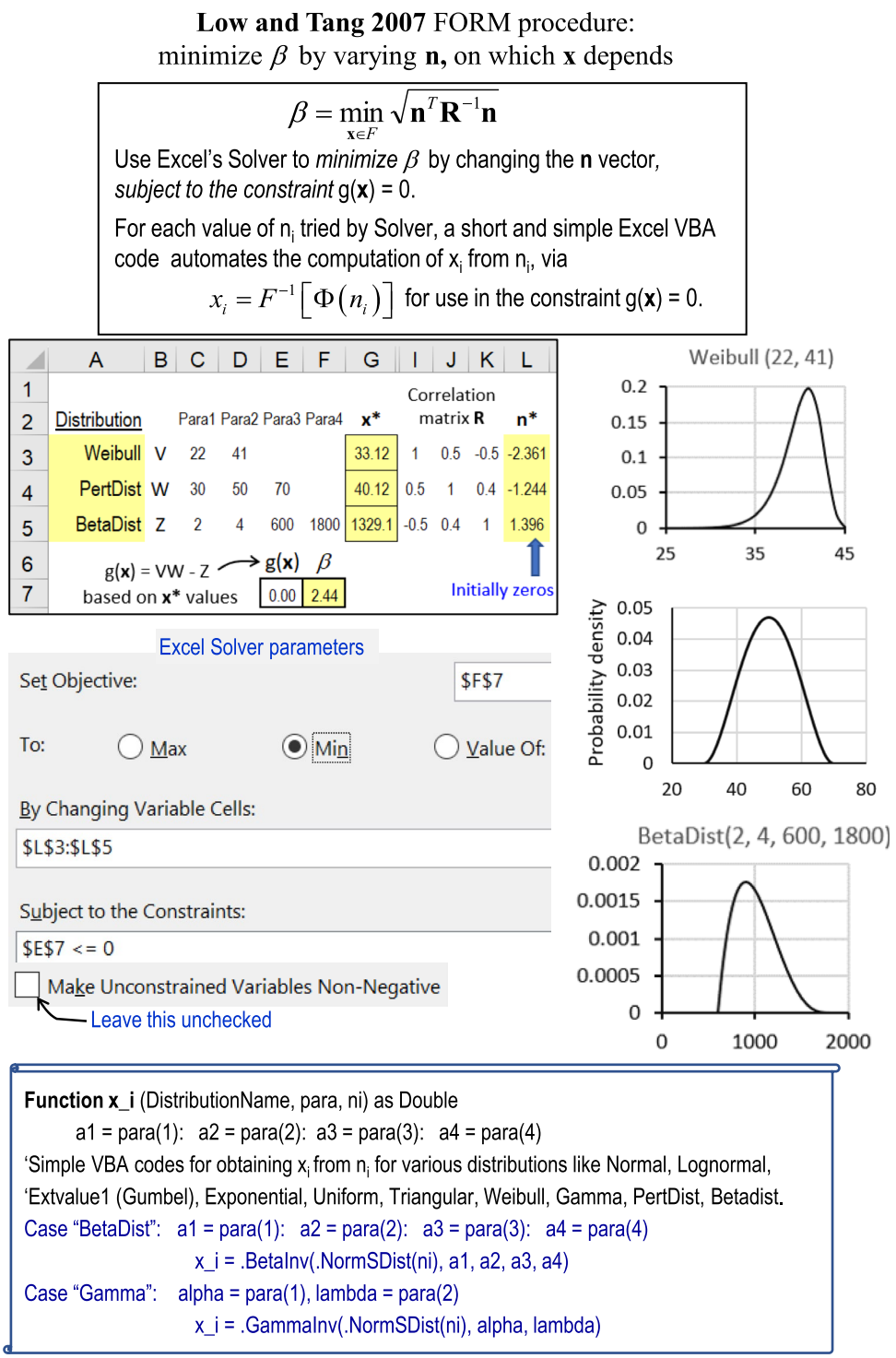

Fig. 1 The efficient Low and Tang Excel procedure for FORM, with more succinct VBA code for getting x_i from n_i made possible by recent Excel functions for BetaInv and GammaInv, as shown in the first figure of the Appendix

different, namely on the integrated use of FORM, direct MCS, Importance sampling (IS), and SORM, where the design point located by FORM becomes the logical center of IS, and the "exact" failure probability from MCS, IS, or SORM allows a revised design much closer to the target failure probability. In this way, the merits of FORM, MCS, IS, and SORM complement one another.

One needs to appreciate the ease of moving from the **n** space (e.g., Fig. 1) to the rotated **u** space (in the classical FORM method) to understand the simple extensions of FORM to MCS, IS and SORM in the examples below. The vectors **n** and **u** can be obtained, one from the other, using the equations below (e.g., Low et al. 2011):

$$\mathbf{n} = \mathbf{L}\mathbf{u} \tag{5a}$$

and

$$\mathbf{u} = \mathbf{L}^{-1}\mathbf{n}, \tag{5b}$$

in which $\mathbf{L}$ is the lower triangular matrix of the Cholesky decomposition of the correlation matrix $\mathbf{R}$. The lower triangular matrix $\mathbf{L}$ is related to $\mathbf{R}$ by $\mathbf{L}\mathbf{L}^T = \mathbf{R}$, where superscript T denotes the transpose of a matrix. The matrix $\mathbf{L}$ can be obtained easily using a very short Excel VBA code for Cholesky decomposition which is available in the public domain.

Only when the random variables are uncorrelated is $\mathbf{n} = \mathbf{u}$, because then $\mathbf{L}^{-1} = \mathbf{L} = \mathbf{I}$ (the identity matrix). In general $\mathbf{n}$ is not equal to $\mathbf{u}$.

1.2 More Accurate Failure Probability Using MCS, Importance Sampling, and SORM

This study shows that one can couple any of the following three methods (easily extended from the Excel FORM template) to obtain near-exact P_f in a revised design. The Appendix explains the extension for the simple $g(\mathbf{x}) = VW - Z$ case in Fig. 1. The procedure is the same for complicated cases like the reinforced pentahedral blocks in later sections.

(1) MCS with sampling emanating from the mean-value point. Setting up MCS requires only one more column to the right of the **n*** column in the FORM template of Fig. 1, as shown in Fig. 10 of the Appendix.
(2) Importance Sampling (IS) near the FORM design point, and achieving converged failure probability with a much smaller sample size than MCS. Setting up IS requires 3 additional columns in the FORM template, as shown in Fig. 11 of the Appendix.
(3) SORM to estimate curvatures at the FORM design point, and revised FORM P_f accordingly to a SORM P_f. Setting up SORM requires 5 additional columns in the FORM template, as shown in Fig. 12 of the Appendix.

MCS and IS for near-exact P_f estimation are easily extended from the Excel FORM template, with simple VBA codes, while SORM requires more VBA codes. In return, their near-exact P_f values enable a much more accurate re-design via FORM, in the single loop FORM–MCS–FORM design procedure for cases with multiple failure domains. The much faster IS and SORM can be used instead of MCS for cases with a dominant single failure mode, as illustrated next in an interesting case where an inclined load is revealed by FORM as actually playing the role of resistance.

2 Foundation on Rock Containing a Planar Discontinuity

2.1 Deterministic Model Based on Limit Equilibrium Considerations

Figure 2a shows the forces acting on a foundation on rock containing a planar discontinuity dipping out of slope face. The factor of safety against sliding on the discontinuity plane is the ratio of available resistance on the discontinuity plane, $cA + N' \tan\phi$, to the sliding force $Q_{sliding}$:

$$F_S = \frac{cA + N' \tan\phi}{Q_{sliding}}, \tag{6}$$

where N′ (the force perpendicular to the discontinuity plane) and the destabilizing $Q_{sliding}$ force are determined by the two equations below:

$$N' = (Q_{1v} + W)\cos\psi_p - (Q_{1H} + aW)\sin\psi_p - V\sin(\psi_p - \psi_v) - U + T\sin(\psi_T - \psi_p) + Q_2\sin(\psi_{Q2} - \psi_p), \tag{7}$$

$$Q_{sliding} = (Q_{1v} + W)\sin\psi_p + (Q_{1H} + aW)\cos\psi_p + V\cos(\psi_p - \psi_v) + T\cos(\psi_T - \psi_p) + Q_2\cos(\psi_{Q2} - \psi_p), \tag{8}$$

in which the symbols are as defined by the annotated inset at the top right of Fig. 2.

The deterministic analysis in Fig. 2b indicates that when an active bolt force T of 8 MN is applied over a 5 m width (out of plane), the factor of safety against sliding is 1.69, in agreement with Wyllie (1999, p195). If bolt force is zero, the factor of safety is 1.28.

For the given bolt force, Excel Solver indicates that a maximum F_s of 1.87 is obtained when ψ_T is 202.9°, which means 22.9° above horizontal, that is, 17.1° above the discontinuity plane. Wyllie aptly noted that it is, however, easier to drill and grout in a direction below horizontal.

2.2 Statistical Inputs

The global (or lumped) factor of safety as defined by Eq. 6 are typically based on mean values of the parameters (c, ϕ, Q_1, Q_2, a, W, ψ_p, …), and conveys no information on the chance of failure (defined by $F_s \le 1.0$). As an alternative, RBD via FORM can be conducted, based not only on the mean values but also the uncertainty of the input parameters. That the outcome of probability-based design depends on the inputs characterizing uncertainties is discussed in Sect. 6.

Figure 3a shows the simple template for RBD via FORM using the Low and Tang (2007) computational approach. The ten random variables are Q_{1V}, Q_{1H}, Q_2, T, a, W, h_w, c, ϕ

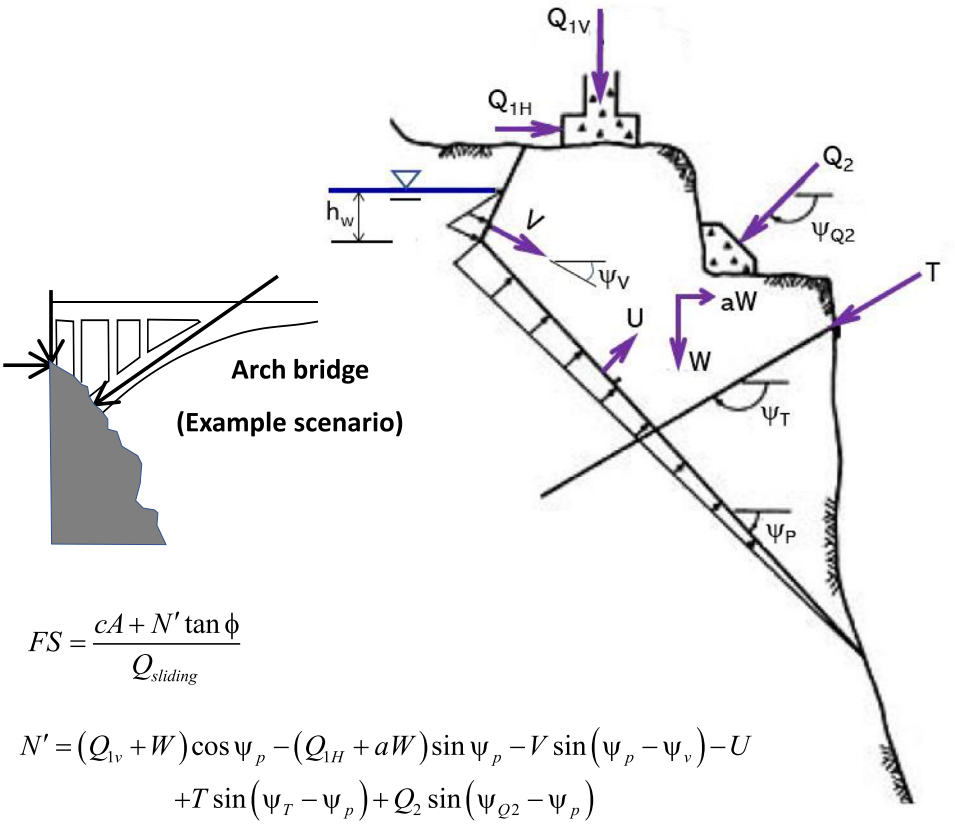

$$FS = \frac{cA + N' \tan\phi}{Q_{sliding}}$$

$$N' = (Q_{1v} + W)\cos\psi_p - (Q_{1H} + aW)\sin\psi_p - V\sin(\psi_p - \psi_v) - U + T\sin(\psi_T - \psi_p) + Q_2\sin(\psi_{Q2} - \psi_p)$$

$$Q_{sliding} = (Q_{1v} + W)\sin\psi_p + (Q_{1H} + aW)\cos\psi_p + V\cos(\psi_p - \psi_v) + T\cos(\psi_T - \psi_p) + Q_2\cos(\psi_{Q2} - \psi_p)$$

(a)

Example: A bolt force of 8 MN (for a 5 m width into the paper) achieves a factor of safety 0f 1.69, given the data below. (If bolt force T is zero, the FS is 1.28.)

Q_{1V}	Q_{1H}	Q_2	T	α	W	A	h_w	γ_w	L
5	2	30	8	0.1	30	190	3	0.0098	5
MN	MN	MN	MN		MN	m^2	m	MN/m^3	m

	ψ_{Q2}	ψ_T	ψ_p	ψ_v	cohesion c	ϕ'	U	V
	130	160	40	20	0.025	30	2.793	0.235
radians	2.269	2.793	0.698	0.349	MPa	(°)	MN	MN

N'	Q_{resist}	$Q_{sliding}$	FS
57.65	38.04	22.55	1.69

(b)

Fig. 2 **a** Forces acting on a foundation on rock containing a planar discontinuity dipping out of slope face (*top-right inset after* Wyllie 1999). **b** Example deterministic evaluation of the factor of safety FS, inputs after Wyllie (1999)

ψ_p ,which have been defined in the top-right inset of Fig. 2a. Bounded non-Gaussian distributions are used.

In the *bounded* beta distribution BetaDist(λ_1, λ_2, min, max) used for seven of the ten random variables in Fig. 3a, λ_1 and λ_2 are shape parameters which can define various shapes for the beta distribution. When $\lambda_1 = \lambda_2$, the beta distribution is symmetric (as in the *unbounded* normal distribution).

The following established relationships are useful to keep in mind:

N'	Q_{resist}	$Q_{sliding}$	FS	g(x)	β
51.67	28.65	28.65	1.00	0.00	3.001

		x*	para1	para2	para3	para4	n*	μ	σ
BetaDist	Q_{1v}	5.108	7.5	7.5	3	7	0.21	5.000	0.500
BetaDist	Q_{1H}	2.047	7.5	7.5	1.2	2.8	0.22	2.000	0.200
PERTDist	Q_2	27.39	24	29	41		-0.81	30.17	3.089
BetaDist	T	6.953	7.5	7.5	4.392	10.248	-0.48	7.32	0.732
PERTDist	α	0.199	0	0.1	0.3		1.37	0.117	0.055
BetaDist	W	31.08	7.5	7.5	18	42	0.34	30.00	3.000
PERTDist	h_w	3.31	0	3	5		0.43	2.833	0.936
BetaDist	c	0.027	7.5	7.5	0.005	0.045	0.37	0.025	0.005
BetaDist	ϕ	24.70	7.5	7.5	18	42	-1.77	30.00	3.000
BetaDist	ψ_p	42.38	7.5	7.5	32	48	1.16	40.00	2.000

Correlation matrix **R**

	Q_{1V}	Q_{1H}	Q_2	T	α	W	h_w	c	ϕ	ψ_p
Q_{1V}	1	0.5	0	0	0	0	0	0	0	0
Q_{1H}	0.5	1	0	0	0	0	0	0	0	0
Q_2	0	0	1	0	0	0	0	0	0	0
T	0	0	0	1	0	0	0	0	0	0
α	0	0	0	0	1	0	0	0	0	0
W	0	0	0	0	0	1	0	0	0	-0.5
h_w	0	0	0	0	0	0	1	0	0	0
c	0	0	0	0	0	0	0	1	-0.5	0
ϕ	0	0	0	0	0	0	0	-0.5	1	0
ψ_p	0	0	0	0	0	-0.5	0	0	0	1

(a)

Note: Cell A in Fig. 2b contains the formula $A = 190 \times \sin 40° / \sin \psi_p$

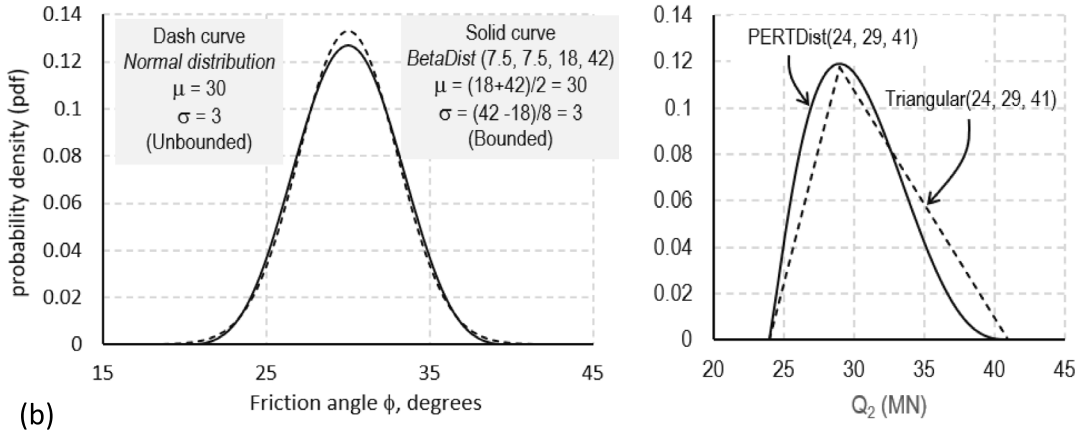

(b)

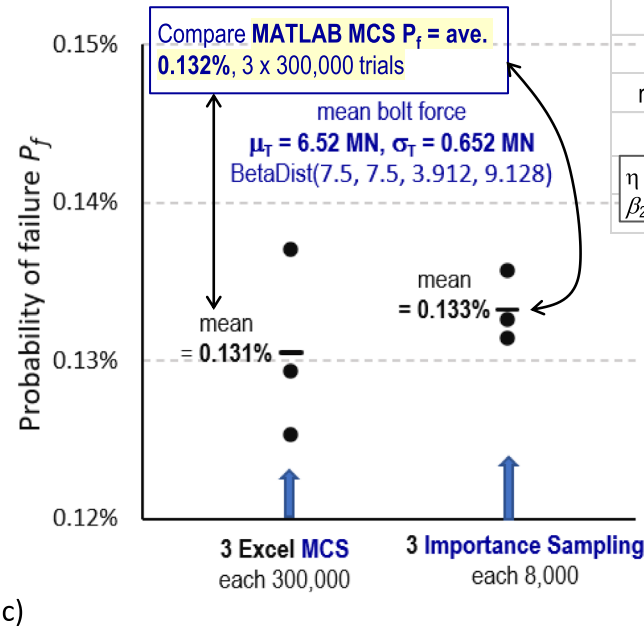

	FORM → IS → FORM → IS			
β =	3.001		2.84	
mean T =	7.32 MN		6.52 MN	
P_f =	0.134%	0.0766%		0.133%

η = 0.134%/0.0766%, β_2 = NormSInv(1 − ηP_{target}) = 2.84

≈ P_{target} of 0.13%

SORM formulas	$P_{f,SORM}$
Tvedt	0.139%
Hohenbichler_Rackwitz	0.141%
Koyluoglu_Nielsen	0.141%
Cai_Elishakoff	0.138%
Hong(P_3)	0.139%
Hong(P_4)	0.140%
AVERAGE	**0.140%**

(c)

Fig. 3 **a** RBD of mean bolt force (μ_T) for a target reliability index (β); **b** Beta distribution of ϕ and PERT distribution of Q_2; **c** Revised design of mean bolt force of 6.52 MN obtains a P_f of 0.133% based on IS, about equal to the target P_f of 0.13%

When $\lambda_1 = \lambda_2 = 7.5$ in the beta distribution BetaDist(λ_1, λ_2, min, max),

$$\text{Mean value} \quad \mu = (\min + \max)/2, \tag{9a}$$

$$\text{Standard deviation} \quad \sigma = (\max - \min)/8, \tag{9b}$$

$$\min = \mu(1 - 4 \times c.o.v.) = \mu - 4\sigma, \tag{9c}$$

$$\max = \mu(1 + 4 \times c.o.v.) = \mu + 4\sigma, \tag{9d}$$

where *c.o.v.* is the coefficient of variation ($=\sigma/\mu$).

The μ and σ values are shown under the eponymous columns in the middle of Fig. 3a. Figure 3b compares BetaDist (7.5, 7.5, 18, 42) for the friction angle ϕ, for which $\mu = 30$ and $\sigma = 3$ by Eqs.9a and 9b, with the normal distribution N(30, 3).

The 3-parameter PERT (also called beta-PERT) distribution, PERTDist(min, mode, max), is used for random variables Q_2, a and h_w in Fig. 3a. The mean μ and standard deviation σ of PERTDist(.) can be calculated from the following established equations:

$$\mu = \frac{\min + 4 \times \text{mode} + \max}{6}, \tag{10a}$$

$$\sigma = \sqrt{\frac{(\mu - \min)(\max - \mu)}{7}}. \tag{10b}$$

Figure 3b compares the PERT distribution with the triangular distribution for the inclined load Q_2.

The loads Q_{1V} and Q_{1H} are assumed to be positively correlated with a correlation coefficient equal to 0.5, and cohesion c and friction angle ϕ of the discontinuity plane are negatively correlated with a correlation coefficient equal to −0.5, as shown in the correlation matrix **R**. Also, the weight W will be larger when the discontinuity inclination angle ψ_p (Fig. 2a) is smaller, hence W and ψ_p are assumed negatively correlated with $\rho_{W\psi p} = -0.5$. The area (A) of discontinuity plane in Fig. 2b is 190 m^2 when $\psi_p = 40°$. In probabilistic analysis, area A will vary according to $A = 190 \times \sin 40° / \sin \psi_p$ as ψ_p changes, assuming the discontinuity plane connects with the tension crack at the same constant elevation.

2.3 Reliability-Based Design (RBD) via FORM and Insights Provided by the FORM Design Point

The RBD-via-FORM procedure in Fig. 3a is similar to Fig. 1. It is easily linked to the deterministic set-up of Fig. 2b by replacing the numerical values of Q_{1V}, Q_{1H}, Q_2, T, a, W, h_w, c, ϕ, ψ_p in Fig. 2b with cell addresses which point to the cells under the **x*** column in Fig. 3a. The deterministic formulation is also needed in the performance function g(**x**) at the top of Fig. 3a, expressed as:

$$g(\mathbf{x}) = Q_{resist} - Q_{sliding} \tag{11a}$$

Or

$$g(\mathbf{x}) = \frac{Q_{resist}}{Q_{sliding}} - 1. \tag{11b}$$

Equations 11a and 11b are mathematically equivalent when $g(\mathbf{x}) = 0$.

Initially the **n*** column values in Fig. 3a were zeros. Excel Solver was then invoked (as in Fig. 1), to minimize the β cell, by changing the **n*** column values, subject to the constraint that the g(**x**) cell is equal to zero. A mean bolt force (μ_T) of 7.32 MN (over a 5 m width) was found to be required to achieve a β of 3.001 (≈ 3.0, typical target for ULS), as shown in Fig. 3a under the column labeled **μ**.

The ten **x*** values represent the first point of contact with the limit state surface (defined by $g(\mathbf{x}) = 0$) when an equivalent hyper-ellipsoid expands from its equivalent normal mean-value point, as explained in connection with Eq. 2. The point represented by the **x*** values which render $g(\mathbf{x}) = 0$ is the design point (or checking point), also referred to as the most probable point (MPP) of failure.

The following are noteworthy:

(i) When the **n*** values are initially zeros, the g(**x**) cell displays a positive value. This means that the mean-value point is in the safe domain; only then can the reliability index (β) value obtained by Excel Solver be regarded as a positive reliability index.

(ii) The values of the sensitivity indicators under the **n*** column are positive for Q_{1V} and W, being 0.21 and 0.34, respectively. Both are destabilizing load entities (hence positive n* values), and both have the same coefficient of variation of 0.1. If W is independent, its much bigger mean value 30 MN relative to the mean value of 5 MN for Q_{1V} would make its sensitivity indicator (n*) value even higher. But being negatively correlated with ψ_p (n* value = 1.16 in Fig. 3a) restrains the n* value of W. (Correlated sensitivities are demonstrated and explained in Low (2020)).

(iii) A significant revelation from FORM is the negative sensitivity indicator value of -0.81 (under the **n*** column) for *load* Q_2. Its design value (under the **x*** column) is 27.39 MN, a decrease from its mean value of 30.17 MN (under the column labeled **μ**). This reveals the resistance nature of "load" Q_2 with respect to sliding along the discontinuity plane. Designers not aware of this might multiply Q_2 by a load factor bigger than 1, heading in a wrong direction. Had Q_2

acted in a vertical direction, it will be a *load* like Q_1 and W. In other directions between vertical on the one hand and perpendicular to the discontinuity plane on the other, it may not be clear to the designer whether to treat it as a load or a resistance. FORM will resolve such ambiguous load–resistance duality automatically.

(iv) When considering the bearing pressure on the pad or intact rock acted on by Q_2, the load Q_2 should of course be multiplied by a load factor greater than 1.0.

(v) The revelation by FORM in (iii) could have been perceived by a deterministic designer who notes that the value of 130° for ψ_{Q2} means that Q_2 is perpendicular to the discontinuity plane. It increases the normal force N and hence acts like a resistance. This can be verified deterministically (via Fig. 2b), by varying the magnitude of Q_2. Also, if $\psi_{Q2}=90°$, a Q_2 value of 30 MN is a destabilizing vertical load, like Q_{1v}, causing the F_s value to drop from1.69 to 0.81. However, deterministic perception of such underlying subtleties may not be straightforward. FORM automatically reveals such subtleties and offers other insights and information at the MPP of failure. Hence, it is beneficial to conduct FORM in tandem with partial factor design approaches like Eurodoce 7 and LRFD. (Simpson (2007) discussed the different ways of combining partial factors in the three design approaches (DA) in Eurocode 7, and the merits of Design Approach 1 (DA1) relative to DA2 and DA3.) FORM automatically reveals the sensitivity of the input parameters, and the calculation procedure is impartial toward biases between DA1, DA2, and DA3.

(vi) The absolute values under the column labeled **n*** suggest that the critical parameters (for this case and the assumed statistical inputs) are friction angle ϕ, horizontal earthquake acceleration coefficient a, inclination angle ψ_p of the discontinuity plane, and Q_2, in decreasing order of significance.

(vii) The design value of c (0.027 MPa), under the x* column, automatically found by FORM, is slightly *above* its mean value of 0.025 MPa. This is due to its being negatively correlated with the more pivotal parameter ϕ (the design value of which, 24.70°, is 1.77 times its *equivalent normal* standard deviation *below* its *equivalent normal* mean. The values of sensitivity indicators can be affected (logically) by parametric correlations, as explained in Low (2020) in another context. In this case, the mean value of $N' \tan \phi$ is several times the mean value of cA, causing the design value of cA to be dragged upwards as the design value of ϕ decreases significantly below its mean.

2.4 Revised Design of Mean Reinforcing Force μ_T via FORM–IS–FORM

The failure probability based on FORM reliability index (Eq. 1) is approximate when the LSS is nonplanar and/or the random variables obey non-normal distributions. Having obtained a required design of mean bolt force $\mu_T=7.32$ MN (over a 5 m width) for a β of 3.001 in Fig. 3a, it is desirable to check the accuracy of $P_f \approx \Phi(-3.001)=0.134$, and to get a new design mean bolt force of μ_T that satisfies the target P_f of 0.13% more closely, as illustrated below.

Section 1.2 and Fig. 10 in the Appendix present the simple extension of the FORM template to MCS, IS, and SORM, each of which can be coupled with FORM to converge to a target failure probability in the single loop FORM–MCS–FORM. Of particular efficiency are IS and SORM (instead of MCS) for cases with a dominant single failure mode (e.g., Fig. 3), as illustrated in the steps below:

(i) For the RBD-via-FORM design in Fig. 3a, importance sampling (IS) on the FORM design point indicates a failure probability of 0.0766%, significantly lower than the P_f of 0.134% based on Eq. 1 for the β value of 3.001 in Fig. 3a.

(ii) A new target β (different from the original target β of 3.0) is calculated from the following equation:

new $\beta_2 = \Phi^{-1}\left(1-\frac{0.134\%}{0.0766\%}\times 0.13\%\right) = 2.84$, with the aim of target P_f of 0.13%.

In Microsoft Excel, this is $\beta_2 = NormSInv\left(1-\eta p_T\right)$ η = 0.134/0.0766.

(iii) RBD via FORM obtains a new mean bolt force $\mu_T=6.52$ MN that achieves the new β_2 in (ii).

(iv) It is verified in Fig. 3c (left) by Excel MCS, Excel IS and MATLAB MCS that the new mean bolt force of $\mu_T=6.52$ MN obtains the small target P_f of around 0.13%. SORM indicates a P_f of 0.14%.

The above-coupled FORM and near-exact P_f methods are summarized by the following expressions:

$$\beta_2 = \Phi^{-1}\left(1-\frac{\Phi(-\beta_1)}{P_{f1}}P_{target}\right), \tag{12a}$$

followed by verification to checkthat MCS (or IS) $P_{f2} = P_{target}$. (12b)

The P_{f1} in the denominator of Eq. 12a can be evaluated by one of three methods, as follows:

(Option 1) FORM–**MCS**–FORM, obtaining β_1, P_{f1}, β_2, (13)

(Option 2) FORM−**IS**−FORM, obtaining $\beta_1,\ P_{f1}, \beta_2$, (14)

(Option 3) FORM−**SORM**−FORM, obtaining $\beta_1,\ P_{f1}, \beta_2$. (15)

Option 1 must be used (i.e., using MCS to determine P_{f1}) if there are multiple failure domains, as in Sects. 4.2 and 5.1 later where sliding mode can be along both planes, or along one of the two planes.

Options 2 and 3 are faster than Option 1, and either can be used if there is a single dominant failure mode, as in Fig. 2 where the sliding mode is down the discontinuity plane. (Option 3, in which SORM is used to determine the P_{f1} in Eq. 12a, was suggested in Low and Einstein (2013, Eq. 15)).

The verification (Eq. 12b) can be done using the faster IS or SORM (as in Fig. 3c) if there is a single dominant failure mode. Otherwise MCS must again be used for P_{f2}, as in Sect. 5.1.

Figure 3c shows that three Importance Sampling each of 8,000 trials show much smaller scatter than three direct MCS each of 300,000 trials. This is because the center of importance sampling is at the FORM design point (i.e., the MPP of failure located by FORM), whereas in direct MCS the samples emanate from the mean-value point, and require larger sample size than IS.

The next section applies the coupled FORM and importance sampling method to design the reinforcing force for a potentially unstable rock slope in Hong Kong. Other derisking measures and the final option adopted will be mentioned.

3 FORM–IS–FORM Procedure for a Failure Probability of 0.5% of a Hong Kong Slope

A rock slope adjacent to the Sau Mau Ping road in Kowloon of Hong Kong was analyzed in Hoek (2023) using MCS. Hencher et al. (2011) also mentioned this case. The granitic block above the exfoliation joint (sheet joint) has a height H of 60 m, Fig. 4a. Resistance against sliding of the block along the sheet joint derives from the shear strength parameters of friction angle ϕ and cohesion *c*. The destabilizing forces are the weight W of block, water forces U and V on the discontinuity planes, and earthquake-induced horizontal force αW. Various derisking measures were mentioned in Hoek (2023), including drainage, external reinforcing force, and slope re-profiling. The risk of the block sliding along the sheet joint was finally eliminated by removing the block (Hoek 2023), although stabilization by bolt force was considered up to the last stage.

What follows is this paper's new contribution to probability-based design via coupled FORM and importance sampling for the design of bolt force for the Sau Mau Ping slope, aiming at 0.5% failure probability against sliding of the block. Hoek's MCS assumed (for simplicity) the five random variables ϕ, c, z, z_w, and α to be independent, but both Hoek (2023) and RocScience (2002) mentioned that cohesive strength generally drops as the friction angle rises and vice versa. Also, Hoek (2023) discussed concerns about uncertain long-term durability and quality of installed reinforcing force. Hence in what follows, c and ϕ are modeled by a negative correlation of − 0.5, and the uncertainty of the (active) reinforcing force T is characterized by a c.o.v. of 0.1. The variables T, ϕ, c, and z are normally distributed, while z_w/z and α obey the highly skewed truncated exponentials. The probability distributions of the five random variables ϕ, c, z, z_w/z, and α in Fig. 4b follow those used by Hoek (2023), which also discussed the reasoning behind the choice of the probability distribution functions.

The negative correlation coefficient of -0.5 between ϕ and *c* shown in the top left of the 6-by-6 correlation matrix **R** in Fig. 4b means that low values of cohesion *c* tend to occur with high values of friction angle ϕ, and vice versa. In addition, one may logically infer that the tension crack depth z and the extent to which it is filled with water (as characterized by the ratio z_w/z) are also negatively correlated. This means that shallower crack depths tend to be water-filled more readily (i.e., z_w/z ratio will be higher) than deeper crack depths, consistent with the scenario suggested in Hoek (2023) that the water which would fill the tension crack in this Hong Kong slope would come from direct surface run-off during heavy rains. For illustrative purposes, a negative correlation coefficient of -0.5 is assumed between z and z_w/z, as shown in entries R_{45} and R_{54}, where R_{ij} denotes entry in row *i* and column *j* of the correlation matrix **R** in Fig. 4b. Even though there are no data to quantify this correlation between z and z_w/z, it is still useful to explore possible correlations to get a feel for its influence on the reliability index. This is a sensible approach commonly applied in engineering practice for important but not well-characterized parameters.

When there is no reinforcing force, i.e., $\mu_T = 0$, the reliability index obtained by Excel Solver is $\beta = 1.887$, implying a probability of failure of about 3%, based on $P_f = \Phi(-\beta)$, which is unacceptably high. (For uncorrelated random variables, and with $\mu_T = 0$, the reliability index is 1.556, with FORM $Pf = \Phi(-\beta) = 6\%$, compared with 6.5% from importance sampling, virtually the same as the P_f of 6.4% using MCS by Hoek (2023)).

Figure 4b, c shows that a mean reinforcing force (μ_T) of 123 tons/m is required to obtain the target failure probability of about 0.5%, after revising the design of μ_T twice based on Eqs. 12 and 14.

Hoek (2023) rightly noted that the permissible failure probability (target P_f) can be higher if the consequence of failure is low, and lower if the consequence of failure is high.

Fig. 4 Coupled FORM and Importance Sampling (IS) applied to the Sau Mau Ping slope of Hong Kong, for a target failure probability of 0.5%

$$F_s = \frac{cA + N' \tan\varphi}{W\left(\sin\psi_p + \alpha\cos\psi_p\right) + V\cos\psi_p - T\sin\theta}$$

$$N' = W\left(\cos\psi_p - \alpha\sin\psi_p\right) - U - V\sin\psi_p + T\cos\theta$$

$$W = 0.5\gamma H^2\left(\left(1-\left(\frac{z}{H}\right)^2\right)\cot\psi_p - \cot\psi_f\right)$$

$$A = \left(H - z\right)/\sin\psi_p$$

$$U = 0.5\gamma_w z_w A \qquad V = 0.5\gamma_w z_w{}^2$$

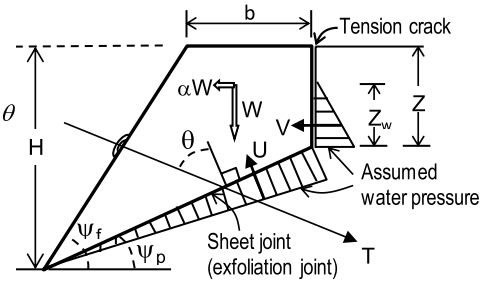

Sau Mau Ping slope of Hong Kong
Ref. Hoek (2007, 2023), Wyllie (2018), Hencher et al. (2011),

(a)

H	ψf	ψp	γ	γw	T	θ	ϕ	c	z	zw	α	Fs	g(x)	β
60	50	35.0	2.6	1	121.4	55	31.0	8.654	13.7	9.96	0.12	1.00	0.00	2.398

A	W	U	V	N'tanϕ	c*A	Denom
80.80	2411	402.2	49.56	867.0	699.3	1566.3

Units: meter, tonne, tonne/m², tonne/m³

u* needed by Importance Sampling

		Para1	Para2	Para3	Para4	x*	Correlation matrix **R**						n*	-n/β	u*
Normal	T	**123.0**	12.3			121.4	1	0	0	0	0	0	-0.127	0.053	-0.127
Normal	ϕ	35	5			30.98	0	1	-0.5	0	0	0	-0.803	0.335	-0.803
Normal	c	10	2			8.654	0	-0.5	1	0	0	0	-0.673	0.281	-1.241
Normal	z	14	3			13.65	0	0	0	1	-0.5	0	-0.115	0.048	-0.115
Tr_Exp	z_w/z	0.5	0	1		0.7292	0	0	0	-0.5	1	0	1.213	-0.506	1.334
Tr_Exp	α	0.08	0	0.16		0.1228	0	0	0	0	0	1	1.324	-0.552	1.324

(b) Statistical inputs of ϕ, c, z, z_w, and α after Hoek (2023, Chapter 9)

from Eqs. 12 and 14:

$$\beta_2 = \Phi^{-1}\left(1 - \frac{\Phi\left(-\beta_1\right)}{P_{f1}(IS)}P_{target}\right)$$

$$\beta_3 = \Phi^{-1}\left(1 - \frac{\Phi\left(-\beta_2\right)}{P_{f2}(IS)}P_{target}\right)$$

where P_{target} = 0.5%

β	μT	FORM Pf Φ(–β)	Pf(IS)
2.575	164.5	0.501%	0.277%
2.364	115	0.905%	0.549%
2.398	**123**		**0.51%** ≈ 0.5%

μ_T = 123 tonnes/m achieves β_3 = 2.398
Verification that P_{f3}(IS) is ≈ 0.5% is optional
Each P_f(IS) took about 30 seconds,. 24000 trials each

(c)

For the case in hand, the RBD is most sensitive to the coefficient of horizontal earthquake acceleration α and the ratio z_w/z. The values of the sensitivity indicators of α and z_w/z, under the column labeled **n*** to the right of the **R** matrix, are 1.325 and 1.213, respectively, higher than the absolute values of the other four **n** values.

A reliability-based design via FORM is able to locate the design point case by case, and in the process reflect parametric sensitivities as affected by case-specific limit state surface, statistical inputs, and correlation structure in a way that design based on prescribed partial factors cannot.

SORM can also be used for a near-exact P_f estimation. SORM analysis requires the FORM β value and design point values as inputs, and therefore is an extension dependent on FORM results. Using the Chan and Low (2012) Excel-based SORM, the average P_f(SORM) value of 0.44% was obtained when the 10 sample points for estimating the 5 components of curvature at the design point in the six-dimensional random variable u space are based on sampling grid coefficient k = 1. If the sampling grid coefficient k is 2.0, the average P_f(SORM) is 0.54%.

The above RBD of a reinforced rock slope illustrates that RBD can be used when (i) there are no EC7 recommended partial factors yet (e.g., the parameters z_w/z and α in Fig. 4b), (ii) when the design show context-dependent sensitivities to the underlying parameters which cannot be reflected by fixed partial factors, (iii) when the parameters are statistically correlated based on physical considerations (e.g., between c and ϕ, and between z and z_w/z in Fig. 4b), and (iv) when there is a failure probability which can be higher or lower depending on the consequence of failure or non-performance (for serviceability limit states).

One may note the following connections between EC7 and the RBD example in Fig. 4b:

(1) The design point (the six values under the column labeled $\mathbf{x_i}$*) has the same qualitative meaning as the design point in EC7. However, the FORM design point is the most probable point of failure at the contact point of an expanding equivalent dispersion ellipsoid with the limit state surface (defined by $F_s = 1$) in 6D space, and reflects context-sensitivity and parameter correlations in a way the design point of EC7 cannot; this is because the design point in EC7 is obtained by applying code-specified partial factors to conservative characteristic values.

(2) The sensitivity indicator values of ϕ and c, equal to -0.803 and -0.673 under the **n*** column in Fig. 4b, means that their influence on the design is similar. This outcome is opposite to the foundation on rock with a discontinuity case in Figs. 2 and 3, where the design is much more sensitive to ϕ than c. This context-dependent sensitivity is attributable to N′tanϕ and cA are of comparable magnitude in Fig. 4b (but not in Fig. 3): being of values 867 and 699 at the MPP of failure in Fig. 4b, and 1264 and 802 at the mean-value point. In contrast, in Fig. 2, N′tanϕ is 33.28, much bigger than the value 4.75 of cA, and similar situation (23.79 versus 4.90) in Fig. 3.

Sections 2 and 3 deal with reinforced two-dimensional blocks in rock slope with a discontinuity plane. The next section investigates (first deterministically, then probabilistically) the stability of a bolted and externally loaded pentahedral (five-faced) block formed by two intersecting discontinuity planes, the slope face, the upper crest surface, and an inclined tension crack. Different failure modes need to be considered, including sliding on both discontinuity planes along the line of intersection, or sliding on only one of the two discontinuity planes.

4 Stability of a Reinforced Pentahedral Block Using Vector Analysis and Excel Solver

The stability analysis of polyhedral wedges in rock slopes involves resolution of forces in three-dimensional space. The problem has been extensively treated, for example in Goodman and Taylor (1967), John (1968), Londe et al (1969), Hendron et al (1971), Jaeger (1971), Hoek et al (1973), Hoek and Bray (1981), Wittke (1990), Priest (1993), Goodman (1995), Low (1997), Kumsar et al. (2000), Park and West (2001), Wang et al. (2004), Jiminez and Sitar (2007), Dadashzadeh et al. (2017), Wyllie (2018), Low (2021), and RocScience (2022), for example. The methods used include stereographic projection technique, engineering graphics, vector analysis, response surface method as a bridge between numerical procedure and FORM, and closed form equations. From another perspective, a methodology for quantitative risk assessment of slope hazards in the Canadian Cordillera was presented by Macciotta et al. (2016), with consideration of the uncertainty in the results.

In Appendix 2 of Hoek and Bray (1981), the *comprehensive solution* (hereafter called *H&B Comprehensive*) requires 113 equations based on vectorial procedures (of dot products and cross-products), for analyzing the stability of pentahedral (five-face) blocks in rock slopes containing two intersecting discontinuity planes and a tension crack, a reinforcing bolt force T, and an external load E. A more rapidly implemented "*short solution*" (hereafter called the *H&B Short*) in the same H&B Appendix 2 consists of 20 equations (including three factor of safety equations for three modes of sliding) for analyzing the stability of tetrahedral (four-face) blocks. The *H&B Short* does not allow for tension crack or external forces/loads, and yields the same factor of safety values as the Low (1997, 2021) closed form solution for tetrahedral wedge mechanism without tension crack and external forces/loads.

The link between the pentahedral block (with tension crack) in the *H&B comprehensive* and the tetrahedral block (without tension crack) in the *H&B Short* is L, which is the distance of tension crack from crest, measured along the trace of discontinuity plane 1, Fig. 5. If the value of L (in the *H&B Comprehensive*) is chosen such that the area of tension crack (and height of tension crack) become zero, the *H&B Comprehensive* reduces to a case without tension crack, and, if external load E and reinforcing force T are absent, and if water pressures u_1 and u_2 of the *H&B Comprehensive* corresponds to those of the *H&B Short*, the computed F_s values will be the same, provided the dip directions of planes 3 and 4 are the same or differ by 180° (which renders the crest horizontal, as assumed in the *H&B Short*).

Deterministic questions on pentahedral block from Hoek and Bray (1981, 348, 351), in S.I.units:

1(a) Determine the F for the pentahedral block bounded by the five planes with dip and dip directions and values of H_1,L,c_1, c_2, ϕ_1, ϕ_2, γ and γ_w shown below, for T = 0, E = 0, and $u_1 = u_2 = u_5$ (Eq. 59).

(b) Determine the F_s for T = 0, E = 0, dry slope, and $u_1 = u_2 = u_5 = 0$

(2) As in1(b), except that load E = 35,586 kN. Find the value of F_{min}.

Solution (1a): F = 1.1379
Solution (1b): F = 1.7360

(3) As in 1(a). Determine the minimum tension T_{min} required to increase the factor of safety to 1.5.

Excel Solver is used (instead of Hoek & Bray Eqs. 81-113), to get the worst direction of load E for lowest F in Q2, and the optimum direction for smallest cable/bolt tension T_{min} in Q3 above.

SOLUTION (2) using constrained optimization in Excel-Solver:
Initially $\psi_e = 0$, $\alpha_e = 185$. Excel Solver obtains $F_{min} = 1.037$, $\psi_e = -1.611°$, $\alpha_e = 173.03°$

SOLUTION (3) using constrained optimization in Excel-Solver:

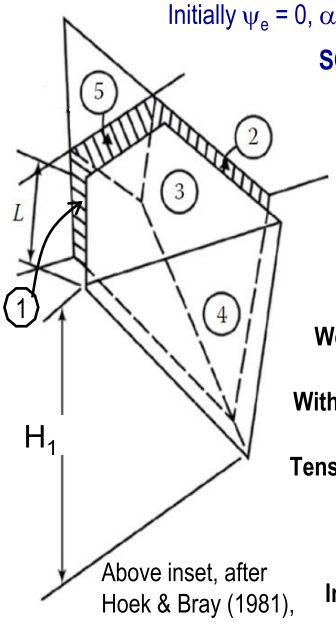

Above inset, after Hoek & Bray (1981), Wyllie (2018)

Plane	1	2	3	4	5	slope face
Dip ψ	45	70	12	65	70	$\eta = 1$
Dip Dir α	105	235	195	185	165	

H_1	L	c_1	c_2	ϕ_1	ϕ_2	γ	γ_w
30.5	12.2	23.94	47.88	20	30	25.1	9.81
m	m	kPa	kPa	0.349	0.524	kN/m^3	kN/m^3

Wedge formed? Yes
With tension crack? TRUE
Tension crack valid? TRUE
Dry Slope? FALSE
Input u_1 & u_2? FALSE

	T × 1	T	E
	15265	15265	0
ψ_t, ψ_e		-6.99	0
α_t, α_e		349.42	0.00

Initially T = 0,
$\psi_t = 0$, $\alpha_t = 338°$
Excel Solver obtains:
T_{min} = 15265 kN,
$\psi_t = -6.99°$, $\alpha_t = 349.42°$

F_{00}	F_1	F_2	F_{12}	F
N.A.	N.A.	N.A.	1.50	**1.50**

Only 80 of the 113 equations in Hoek & Bray (1981) need to be used:

For info:

- There is no tension crack when the height of tension crack (h_5) = 0.
  For the case in hand, this corresponds to a trace length L = 44.95 m, based on Eq. 44 in Hoek & Bray (1981).
- If discontinuity plane 1 is overhanging, vector **a** (first row on the right) has to be multiplied by -1. The same applies to vector **b** if discontinuity plane 2 is overhanging.

	x	y	z	Eq. #
a	0.683	-0.183	0.707	1
b	-0.770	-0.539	0.342	2
d	-0.054	-0.201	0.978	3
f	-0.079	-0.903	0.423	4
f_5	0.243	-0.908	0.342	5
t	-0.182	0.976	0.121	6
e	0.000	1.000	0.000	7
g	-0.561	0.345	0.631	8
g_5	-0.579	0.062	0.575	9
i	-0.319	0.778	0.509	10
j	-0.798	0.055	-0.033	11
j_5	-0.819	-0.256	-0.098	12
.....				.....
.....				44
.....				45

				Eq. #
ψ_i	31.20			46
α_i	157.73	-0.389		47*
			0.183	48
Wedge is formed			0.235	49
			0.293	50
Valid tension crack			26.694	51
			0.444	52*
Areas and weight o			0.428	53*
A_1	517.7			54
A_2	598.0			55
A_5	171.77			56
W	125838			57
.....				.....
.....				79
.....				80

Fig. 5 Deterministic verification of stability analysis of a pentahedral block in rock slope, bounded by two intersecting discontinuity planes (1 and 2), upper ground surface (3), slope face (4), and tension crack (5). (Deterministic questions after Hoek and Bray 1981)

4.1 Verifying with the Deterministic Examples in Pages 348–351 of Hoek and Bray (1981)

Figure 5 shows the deterministic questions on a pentahedral block from Hoek and Bray (1981, p348 & 351), in S.I. units. The solutions for questions 1(a) and 1(b), F = 1.1379 (when planes 1, 2, and 3 are filled with water), and F = 1.7360 (when the three planes are dry), obtained using the first 80 equations in *H&B Comprehensive* formulations, are identical to the F values given in Hoek and Bray (1981).

The solution for question 2 of Fig. 5, obtained readily using the Excel Solver constrained optimization tool, yields the same F_{min} of 1.04 and the same worst direction ($\psi_e = -1.61°$, $\alpha_e = 173.03°$) as those in Hoek and Bray (1981, Eqs. 81–98). In the efficient Excel Solver approach, the initial trial worst direction was (plunge $\psi_e = 0$, trend $\alpha_e = 185°$), where 185° was the dip direction of the slope face. Excel Solver was used to minimize the F cell, by changing (automatically) both the ψ_e and α_e cells. An F value of 1.037 was obtained as the minimum, together with a worst direction of ($\psi_e = -1.611°$, $\alpha_e = 173.03°$).

The solution for question 3 of Fig. 5 was also obtained efficiently using the Excel Solver constrained optimization tool. Initially the value in the T cell was zero and plunge angle $\psi_t = 0$, and the initial trial trend direction (α_t) of T is taken to be opposite to the trend (α_i) of the line of intersection (Eq. 47 in Fig. 5), that is, initial trial value of $\alpha_t = 157.73 + 180$, or 338°. The Excel Solver tool was invoked, to minimize the T × 1 formula cell, by changing (automatically) the three cells of T, ψ_t and α_t, subject to the constraint that the F cell value is 1.50. Excel Solver first reported a converged solution, then, when run a second time, found a solution (T = 15265 kN, $\psi_t = -6.99°$, $\alpha_t = 349.42°$) which is virtually identical to that in Hoek and Bray (Hoek and Bray, 1981, Eqs. 99–113).

(Note: The plunge ψ_I and trend α_i of the line of intersection are calculated from arcsine and arctangent functions, respectively, as given by Eqs. 46 and 47 in Hoek and Bray (1981, Appendix 2) and Wyllie (2018, Appendix III). Arcsine and arctangent can return two principal values. Nevertheless, one can decide the correct trend direction for a downward plunging line of intersection by requiring the trend to be between a right-angle quadrant to the left and right of the dip direction of a *non-overhanging* slope face (i.e., Plane 4 in Fig. 5), or within ± 90° opposite to the dip direction of an *overhanging* slope face.)

4.2 Probability-Based Design of a Reinforced Pentahedral Block via Coupled FORM and MCS

The deterministic case of the Hoek and Bray pentahedral block of Fig. 5 is extended in this section to reliability-based design of the bolt force T for a target probability of failure of 0.1%.

4.2.1 Considerations on Statistical Inputs

The uncertainties and probability distribution of the orientations (ψ_1, α_1, ψ_2, α_2) of discontinuity planes 1 and 2 of Fig. 5 are the same as the SWedge example of RocScience (2002, p41–45) which has the same geometry as the Hoek and Bray example of Fig. 5), namely the standard deviations are 3° for the dip and dip directions of the two discontinuity planes, and normally distributed, as shown in Fig. 6.

Instead of the orientation (dip angle ψ_5, dip direction α_5) of the tension crack, the uncertainty of its trace length L on the crest could have a more significant influence on the probability of failure, because L affects the vertical height h_5 of the tension crack. In the Hoek and Bray water pressure model of "filled fissures", the water pressure increases hydrostatically from zero at the top of the tension crack, to a maximum value at the intersection point between the line of intersection of the two discontinuity planes and the bottom of the tension crack, then decreases linearly to zero at where the line of intersection daylights on the slope face; water pressure is assumed to be zero around the edges of the pentahedral block on the upper ground surface (plane 3) and the slope face (plane 4) in Fig. 5. With this in mind, the length L of 12.2 m in Fig. 5 is treated as mean value, and the standard deviation of L is 0.8 m, obeying the bounded BetaDist (7.5, 7.5, 9, 15.4), as shown in Fig. 6a. This means that the probability density function (PDF) of L is symmetric (as in the normal distribution), but bounded between min and max, and with mean = 0.5*(min + max), and σ = (max − min)/8, (See also Eq. 9 and Fig. 3b; the PDF of BetaDist(α_1, α_2, min, max) can assume various non-symmetric shapes when $\alpha_1 \neq \alpha_2$.).

The height H_1 is also treated as a random variable, obeying the bounded BetaDist (7.5, 7.5, 22.5, 38.5), with a mean value 30.5 m and a standard deviation of 2 m, as shown in row 2 of Fig. 6a.

The bolt force T, to be designed, is also regarded to have some uncertainty, represented by a coefficient of variation (c.o.v., i.e., σ/μ) of 0.1.

The standard deviations of c_1 and c_2 are assumed to be 4 and 8 kPa, respectively, and that of ϕ_1 and ϕ_2 are 2° and 3°, respectively, as shown in the last 4 rows of Fig. 6a.

The cell g(**x**) at the top right of Fig. 6a contains the formula "= F − 1", and the cell β contains the array formula Eq. 3. The 11 random variables in Fig. 6a are assumed to be independent to appreciate their uncorrelated sensitivities; correlated sensitivities are demonstrated and discussed in Low (2020) for a horizontally loaded light-weight structure.

The link between Fig. 5 and Fig. 6 is readily accomplished by replacing the numbers in cells T, H_1, L, ψ_1,

μ	σ		Distrib^n	x*	para1	para2	para3	para4	n*	g(x)	β
		T	Normal	14246.3	14915	1491.5			-0.448	0.000	**2.956**
30.5	2	H_1	BetaDist	33.77	7.5	7.5	22.5	38.5	1.629		
12.2	0.8	L	BetaDist	11.79	7.5	7.5	9	15.4	-0.486		
		ψ_1	Normal	43.20	45	3			-0.600		
		α_1	Normal	107.00	105	3			0.668		
		ψ_2	Normal	67.76	70	3			-0.746		
		α_2	Normal	235.02	235	3			0.005		
		c_1	Normal	21.33	23.94	4			-0.652		
		c_2	Normal	35.54	47.88	8			-1.542		
		ϕ_1	Normal	17.97	20	2			-1.015		
		ϕ_2	Normal	27.98	30	3			-0.672		

(a)

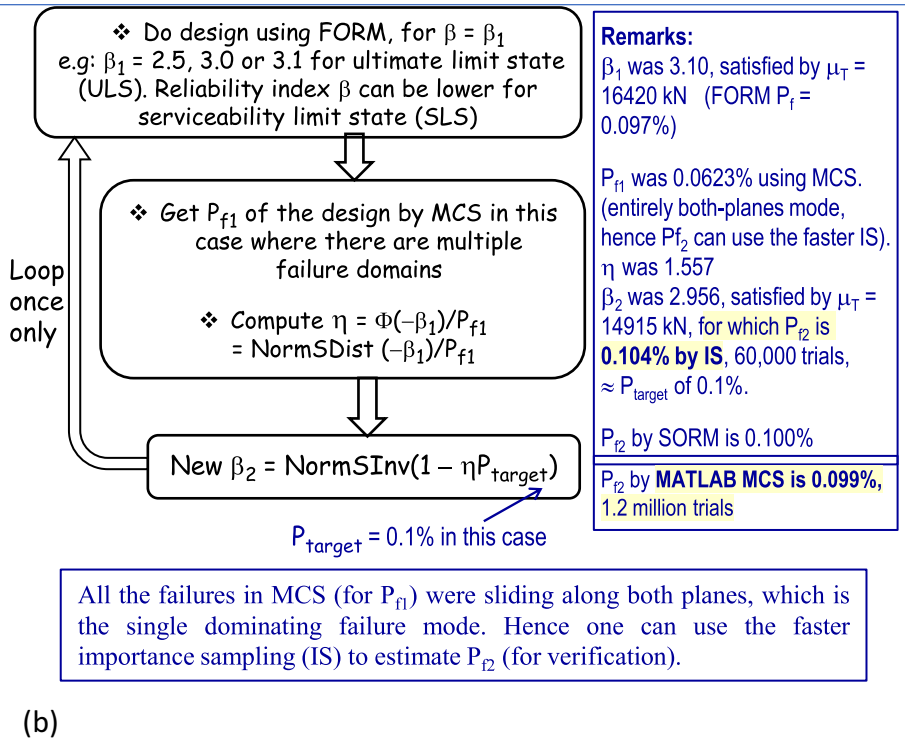

(b)

Fig. 6 RBD of the mean bolt force μ_T of the pentahedral block of Fig. 5, for a target probability of failure (P_{target}) of 0.1%, by coupling FORM and MCS, then FORM and IS

α_1, ψ_2, α_2, c_1, c_2, ϕ_1, and ϕ_2 of Fig. 5 with cell addresses referring to the corresponding cells under the **x*** column in Fig. 6a. The cells in the **x*** column contain the simple function x_i(DistrinutionName, para, ni), which obtains x_i value from n_i value by Eq. 4.

The initial values under the n* column in Fig. 6 were zeros. FORM analysis using Excel Solver was done using different trial mean T values until $\mu_T = 16{,}420$ achieves a target β value of 3.1, corresponding to a FORM P_f of about 0.1%. Three direct MCS each of 400,000 trials were then conducted for this case with multiple failure domains, and yielded an average MCS P_f of 0.0623%, as "remarked" in Fig. 6b. The ratio of $\Phi(-\beta_1)/(\text{MCS } P_{f1})$ then led to a revised target FORM β_2 of 2.956, which was achieved by a μ_T of 14,915 kN, first row of Fig. 6a. All the failure modes in the MCS for P_{f1} were sliding on both planes (which is, therefore, the single dominant failure mode); hence, the verification P_{f2} was done using the much faster importance sampling at the FORM design point of β_2, confirming that, for $\mu_T = 14{,}915$ kN, the failure probability P_{f2} (in 60,000 trials) is 0.104% (nearly the target 0.1%), as remarked in Fig. 6b. Also remarked in Fig. 6b is the P_{f2} of 0.099% obtained by MATLAB MCS in 1.2 million trials.

In this case where there are multiple potential failure modes, direct MCS with sampling emanating from the mean-value point should be conducted first, in case other sliding modes (apart from sliding on both planes in Fig. 5) also contribute non-negligibly to the total failure probability. The faster IS was used only after MCS indicated a dominating failure mode.

The approximate nature of Eq. 1 is again demonstrated in Fig. 6b: the small target P_f of 0.1% was achieved by a FORM β of 2.956, not 3.10.

The absolute values of the sensitivity indicators n_i suggest that, for the given statistical inputs, the three most significant parameters affecting reliability are height H_1 of the pentahedral block, cohesion c_2, and friction angle ϕ_1. When uncorrelated, a negative n* value indicates a resistance parameter (for T, c_1, c_2, ϕ_1 and ϕ_2) and a positive n* value indicates a load parameter. It is also notable that the MPP value of L under the **x*** column (11.79 m) is smaller than its mean value of 12.2 m. Smaller trace length L implies greater tension crack depth and higher water pressures of u_1, u_2 and u_5, but smaller L also reduces the weight of the pentahedral block and the areas A_1 and A_2 on which shearing resistance and water pressures u_1 and u_2 act and increases the area A_5 on which u_5 acts. Compensatory effects are involved, and whether the MPP value of L should be bigger or smaller than its mean value will be resolved automatically on a case-specific basis during the determination of FORM β by Excel Solver. The same automatic FORM resolution of the critical directions in arriving at the MPP of failure (the **x*** values) also applies to the geometrical random variables ψ_1, α_1, ψ_2 and α_2, which interact intricately not merely among themselves in a three-dimensional way but also with the 3D forces acting on the discontinuity planes.

The Hoek and Bray "filled fissures" water pressure model of the pentahedral block in Figs. 5 and 6 implies $u_1 = u_2 = u_5$. We next consider a tetrahedral block without tension crack, in which water pressures u_1 and u_2 on discontinuity planes 1 and 2 can have different values, and more than one failure mode contributes to the failure probability.

5 Probability-Based Design of a Reinforced Tetrahedral Block

A tetrahedral block from Priest (1993, Example 8.4, possibly a site case) is analyzed deterministically in this section, using the *H&B Comprehensive* vectorial procedure in Excel, for comparison with the stereographic-projection-and-equations method in Priest (1993). (Note: The *H&B Short* vectorial procedure cannot be used for this example because there are external loads and the intersection line ("crest") between planes 3 and 4 is not horizontal.)

The deterministic analysis is extended below to a reliability-based design of bolt force for a target failure probability of 0.1%.

As shown in Fig. 7a, a non-overhanging rock slope face of orientation (dip direction/dip angle) 230/60 and its upper ground of orientation 225/05 are intersected by two discontinuities of orientations 203/47 and 287/52, to form a kinematically feasible tetrahedral block. The information on the volume of the block and triangular surface areas of planes 1 and 2 given in Priest (1993) means that the height H_1 is 6.8 m. For the tetrahedral wedge with no tension crack, the trace length L of discontinuity 1 on plane 3 must satisfy the equation $L = Mh/|p|$, so that height h_5 and area A_5 of tension crack are zero, where the entities M, h and p are given by Eqs. 41, 43 and 19 in Hoek and Bray (1981). The equation for L must be entered in the eponymous cell in Fig. 7a, because during subsequent RBD the values of H_1 and the orientations of planes 1 and 3 will change, and the cell labeled L must change accordingly.

In Fig. 7a, the values of cohesions (c_1, c_2), angles of friction (ϕ_1, ϕ_2), and average water pressure (u_1, u_2) of the two discontinuities are as given by Priest (1993). The foundations of a pylon to be sited on the block will exert a force of 180 kN downwards along a line of trend/plunge 168/70, as shown by the values under the column labeled E.

The factor of safety against sliding is calculated to be 1.4966, Fig. 7a, in which the label F_{12} means that the potential mode of sliding is on both planes 1 and 2, along the line of intersection. This example is also analyzed deterministically in SWedge of RocScience (2022, Verification Problem #6, p31-33), which also reports an F_s of 1.4966.

5.1 From Deterministic Analysis to Design of Bolt Force for a Target Failure Probability of 0.1%

The 11 random variables in Fig. 7b are those related to (i) geometry: H_1, dips (ψ_1, ψ_2) and dip directions (α_1, α_2) of the two discontinuities, (ii) water pressure (u_1,u_2) and shear strength parameters of the discontinuities (c_1, c_2, ϕ_1, ϕ_2). Their mean values μ (first column) are the same as those in the deterministic example in Fig. 7a. The values of their standard deviations σ (second column) are illustrative but realistic and within the typical range. All are assumed to follow the 4-parameter bounded BetaDist(λ_1, λ_2, min, max), which is symmetric when $\lambda_1 = \lambda_2$, and, when $\lambda_1 = \lambda_2 = 7.5$, obeys the relationships $\min = \mu - 4\sigma$ and $\max = \mu + 4\sigma$. We already encountered an example of BetaDist (7.5, 7.5, min, max) in Fig. 3b. These bounded symmetric beta distributions are intentionally selected as approximations of the symmetric but unbounded normal distributions, which are not used here because occasional extremely large or extremely small (or negative) values of random numbers generated from normal distributions may cause numerical errors (during MCS

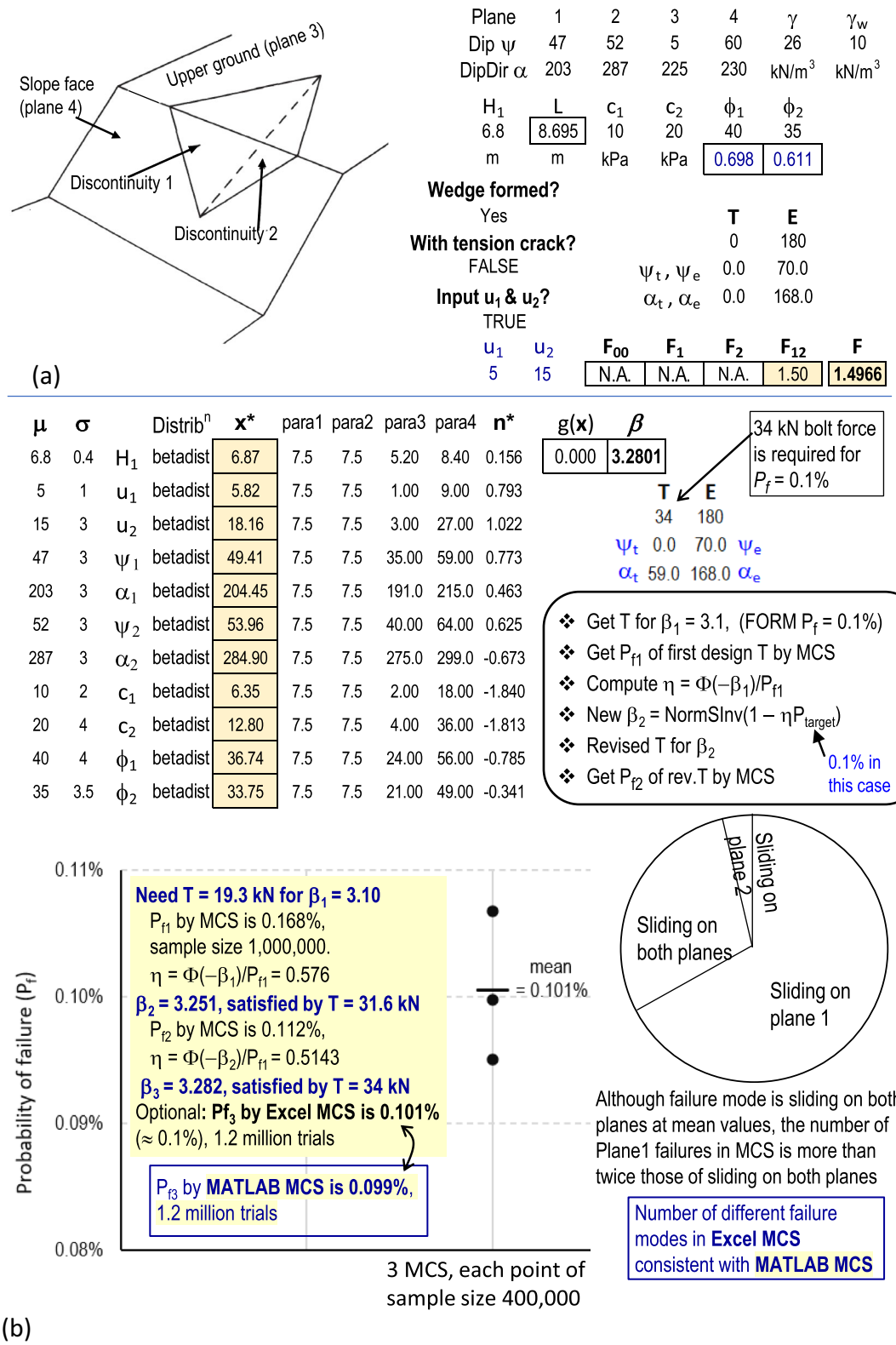

Fig. 7 **a** Deterministic analysis of a tetrahedral block (after Example 8.4 in Priest 1993); **b** RBD of required bolt force T by coupling FORM and MCS.

involving huge sample size of hundreds of thousands) in the *H&B comprehensive* vectorial procedure which has around 100 equations. The deterministic set-up of Fig. 7a is easily linked to the FORM template of Fig. 7b by replacing 11 numerical inputs in the former with cell addresses reading values from the **x*** column in the latter. The performance function g(**x**) is "=F − 1". The β cell contains an array formula as explained in Fig. 1. The 11 random variables are assumed uncorrelated in this illustrative example.

The bolt force T (next to the load E from the foundations of a pylon) in Fig. 7a was zero. It is now required to find the (active) bolt force T for a target failure probability of 0.1%. The bolt force T is taken to act horizontally ($\psi_t = 0$) with a trend direction of 59°, that is, opposite to the trend ψ_i (= 239.4°) of the line of intersection. A first-design T value of 19.3 kN was required to achieve a β of 3.1 using FORM. The FORM P_f of 0.1% by Eq. 1 is approximate. The P_{f1} by MCS was 0.168%, as shown in Fig. 7b bottom left. A revised β_2 of 3.251 was computed from Eq. 12a, which is satisfied by a revised T of 31.6 kN. Three MCS runs each with sample size of 400,000 obtained a P_{f2} of 0.112%, which suggested a β_3 of 3.282, satisfied by a revised T of 34 kN (Fig. 7b). The optional P_{f3} by Excel MCS in 1.2 million trials is 0.101%, which agrees with Pf_3 of 0.099% via MATLAB MCS using the same number of trials.

Measurements obtained from instrumentation and monitoring such as load cells for active anchors (Boon et al. 2015b, 2019) may suggest realistic coefficient of variation (c.o.v.) if the uncertainty in the bolt force is to be modeled. (In Figs. 3 and 6, the c.o.v. of the bolt force T is assumed to be 0.1). Alternatively, numerical analysis may be used to obtain c.o.v. of bolt forces (Boon et al. 2015a).

For cases with multiple failure modes, direct MCS should be done first despite its time-consuming nature and large sample-size requirement when failure probability is small, because MCS can sample into the failure domains of the different failure modes. For the pentahedral case in Figs. 5 and 6, MCS must be used for P_{f1} because of multiple failure domains. The faster IS can be used for verifying P_{f2} only after MCS indicates all failure modes are sliding on both planes. The single dominant failure mode of Fig. 6 should not be presumed, as direct MCS for P_{f1} revealed that for the tetrahedral block in Fig. 7, the number of sliding failures on plane 1 is more than twice that of sliding on both planes, even though the failure mode is sliding on both planes when the random variables are at their mean values. More about this phenomenon in the next section.

5.2 A Tetrahedral Block That Slides on a Single Plane

For the pentahedral block in Fig. 5, the mean-value mode (sliding on both planes) was revealed to be the single dominant mode in the MCS of Fig. 6. For the tetrahedral block in Fig. 7, although the mean-value mode is also sliding along both planes, the more likely failure mode in MCS is sliding on plane 1, with other modes also contributing to failure probability. In contrast, for the tetrahedral block in Fig. 8, the governing sliding mode is along plane 2 for the given water pressures u_1 and u_2, but the sliding mode can change to a different one (along both planes) when the water pressures are different.

The deterministic data in Fig. 8 are the same as Priest (1993, Example 8.5), which compute the F_s using equations and the graphical stereographic projection method. The F = 0.8493 in Fig. 8, obtained using the *H&B Comprehensive* vectorial procedure, is identical to the F value reported by SWedge (RocScience 2022, Verification Problem #7). The "$F_2 = 0.8493$" in Fig. 8 means that the mode of sliding is along plane 2, sliding away from the line of intersection and from plane 1. One may note the factors contributing to this single-plane sliding mode: discontinuity 1 is steep ($\psi_1 = 74°$), and its water pressure ($u_1 = 25$ kPa) is high relative to the water pressure (15 kPa) on the less steep discontinuity 2 ($\psi_2 = 41°$).

Had the slope been dry, with $u_2 = u_2 = 0$, the F_s is 2.3716, and the sliding mode is along both planes.

For other pressures of u_1 and u_2 between the dry scenario and the scenario represented by the data in Fig. 8 (where $u_1 = 25$ kPa, $u_2 = 15$ kPa), the governing sliding mode could be either sliding on both planes, or on plane 2 only. For example, with $u_2 = 15$ kPa, the both-planes mode (i.e., sliding along the line of intersection) governs when $u_1 \leq 21.91$ kPa), and Plane 2 mode governs when $u_1 > 21.91$ kPa. There is an abrupt drop of F at the transition from both-planes mode to the Plane 2 mode, caused by the sudden loss of cohesive resistance c_1A_1 when the block detaches from plane 1. For cases with multiple failure modes (i.e., multiple failure domains), direct MCS (with sampling emanating from the mean-value point) must be used when it is possible that more than one failure mode will contribute toward the total failure probability.

Simpson et al. (2011) reviewed case histories of failures caused by water pressure and the safety provisions related to water pressure in some existing geotechnical codes, including Eurocode 7.

6 Computed Probability of Failure is not Unique nor Intrinsic, but Depends on Inputs

Rock density is an intrinsic and endogenous property of a piece of rock. In contrast, computed failure probability is neither intrinsic nor unique, but depends on statistical inputs. The same limitations to probabilistic approaches

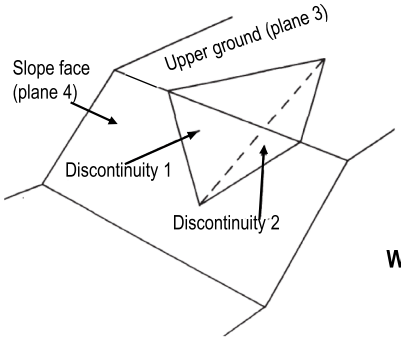

Plane	1	2	3	4	γ	γ_w
Dip ψ	74	41	11	65	25	10
DipDir α	65	186	122	134	kN/m^3	kN/m^3

H_1	L	c_1	c_2	ϕ_1	ϕ_2
6.847	10.49	15	5	32	40
m	m	kPa	kPa	0.559	0.698

Wedge formed? Yes

With tension crack? FALSE

Input u_1 & u_2? TRUE

	T	E
	0	0
ψ_t, ψ_e	0.0	0.0
α_t, α_e	0.0	0.0

u_1	u_2	F_{00}	F_1	F_2	F_{12}	F
25	15	N.A.	N.A.	0.8493	N.A.	0.8493

The above F = 0.8493 agrees with Swedge Verification manual (RocScience 2022, p36)

(a)

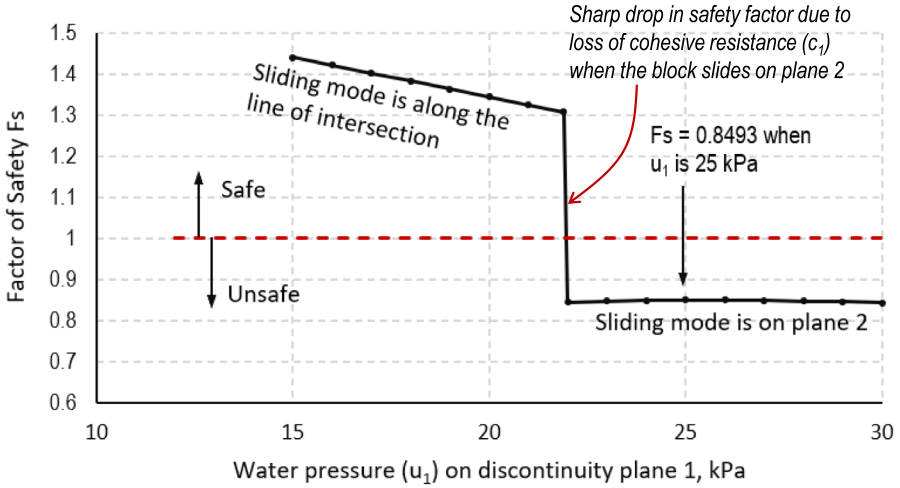

"*… Sliding along plane 2 will occur …. This sliding direction has been 'pushed' slightly away from the line of intersection between the discontinuities largely due to the high water pressure on discontinuity 1. It is likely, however, that as discontinuity 1 opens up, the water pressure will drain away and the block will re-stabilise, perhaps after only a few millimetres of movement.*" Stephen D. Priest (1993, p240)

(b)

Fig. 8 **a** A tetrahedral block that slides on discontinuity 2 when the water pressure (u_1) on discontinuity 1 is 25 kPa (after Example 8.5 in Priest 1993). **b** Factor of safety versus water pressure on discontinuity 1, with $u_2 = 15$ kPa

with respect to approximate inputs, idealized formulations in the performance function, non-exhaustive factors and unknown unknowns also apply to the outputs of deterministic analysis, for example computed F_s and FEM-calculated displacements.

One is reminded of Terzaghi's pragmatic approach of aiming at designs such that unsatisfactory performance is not likely, not aiming at designs which would behave precisely (e.g., not aiming at footing settlement of exactly 25 mm). It is in the same spirit that probability-based-design aims to achieve sufficiently safe design, not at a precise probability of failure. One may note that a EC7 design (or LRFD design) via conservative characteristic/nominal values and code-specified partial factors also aims at a sufficiently safe design by implicit considerations of parametric uncertainties. In contrast, the uncertainties, correlations and probability distributions of random variables are open to view in a probability-based-design. Instead of shunning probabilistic approaches, case-specific scrutiny and counter-suggestions for more reasonable statistical inputs and related

issues in probability-based design are more likely to result in advancements and improvements of the design approach.

A probability-based design requires additional statistical inputs which are not required in a deterministic analysis, but results in richer information pertaining to the performance function and the design point that is missed in a deterministic analysis.

Like F_s, a computed probability of failure is an outcome that will change if the inputs are different. Nevertheless, reliability analysis and probability-based-design are valuable for improving design rationale, resolving ambiguities (e.g., load–resistance duality), and revealing occasional subtleties. Hence, conducting reliability analysis and probability-based-design in tandem with Eurocode 7, LRFD and other design approaches can be enlightening and insightful.

7 Summary and Conclusions

This study provides an efficient Excel template for analyzing the F_s of reinforced and externally loaded pentahedral (five-faced) blocks in rock slopes, based on the first 80 equations of the comprehensive vectorial procedure of Hoek and Bray (1981), which is also in Wyllie (2018). An alternative Excel-Solver procedure is demonstrated, for determining the worst direction of a load and the best direction of a bolt force, in lieu of Hoek and Bray Eqs. 81–113. The deterministic computational procedures in this study are verified against cases in Hoek and Bray (1981), Priest (1993), Wyllie (2018), and RocScience (2002, 2022). This study then extends the deterministic template to RBD of reinforced rock slopes aiming at a small target failure probability (e.g., $P_f = 0.1\%$). Instead of iterative trial designs via repeated MCS alone, this study illustrates the more efficient and time-saving FORM–MCS–FORM design approach, with a second round of MCS for verification if desired. Computed failure probabilities were also verified by comparisons with MCS using MATLAB.

Apart from coupled FORM and MCS for probability-based design of 3D reinforced pentahedral and tetrahedral blocks, this study also demonstrates the automatic resolution of load-resistance duality and case-specific parametric sensitivities of reinforced 2D blocks, including a site case of Hong Kong slope, and other insights and information at the design point provided by FORM. The need for more thoughts in applying load factors is indicated. FORM would facilitate the engineer to verify automatically whether a variable acts as a load or resistance; variabilities in parameters (e.g., relative inclinations) which affect whether a variable is a load or resistance are accounted for.

While it is widely appreciated that FORM P_f is approximate in cases involving nonlinear LSS and non-normal distributions, the coupled FORM–MCS–FORM design procedure is more accurate and efficient than implementing either FORM or MCS by itself alone. It is demonstrated that for cases with multiple failure domains, it is necessary to ascertain the different failure modes with a run of MCS (as in Figs. 6 and 7). The direct MCS in the FORM–MCS–FORM design method can be done using available user-friendly MCS software such as @RISK of palisade.com, SWedge of RocScience.com, MATLAB, or the easy Excel-based direct MCS method (Appendix Fig. 10) for correlated non-normal variates. The Excel-based MCS requires adding only one column to the Low and Tang (2007) FORM template.

When only a single dominant failure mode is involved (e.g., Figs. 2 and 3, and Figs. 4, 5, and 6), one can use the faster importance sampling (IS, centered at the design point provided by FORM), in which case the single design method becomes FORM–IS–FORM. The fast SORM can also be used when only a single dominant failure mode is involved, in which case the method becomes FORM–SORM–FORM. (MCS should be used when it is not clear whether a single dominant mode exists, followed in the verification stage by the faster IS or SORM once the dominant single failure mode has been confirmed by MCS). Given that probabilistic calculations are becoming more prevalent in rock engineering, an understanding of limitations and solutions to overcome these are important. The FORM–MCS–FORM design method (or FORM–IS–FORM for cases with dominant single failure mode) proposed here is useful for probability-based design aiming at a target P_f.

Appendix A

(See Figs. 9, 10, 11, 12).

The more succinct Excel algorithm for obtaining x_i from n_i via $x_i = F^{-1}\left[\Phi\left(n_i\right)\right]$ and the easy extension of the FORM template to Monte Carlo simulation (MCS) are shown in Figs. 9 and 10 below, respectively, for the $g(\mathbf{x}) = VW - Z$ case in Fig. 1 of this paper. The extensions from FORM to importance sampling (IS) and second-order reliability method (SORM) are shown in Figs. 11 and 12 below. The procedures are the same for more complicated cases, for example Figs. 3 and 4 in the paper, which coupled FORM and IS for cases with a single dominant failure mode, and Figs. 6 and 7, which coupled FORM and MCS for cases with multiple failure modes. The procedure can also be applied to cases in which VBA functions and macros are required for evaluating the performance functions $g(\mathbf{x})$.

Fig. 9 More succinct Excel algorithm for obtaining x_i from n_i

```
Function x_i(DistributionName, para, ni) As Double
'Revised by B.K.Low, more succinct for BetaDist, Gamma, and PertDist, n 2023
a1 = para(1):  a2 = para(2):  a3 = para(3):  a4 = para(4)
With Application.WorksheetFunction
Select Case UCase(Trim(DistributionName))
 Case "NORMAL":     x_i = a1 + ni * a2
 Cases LOGNORMAL, TR_EXP, EXTVALUE1,
       EXPONENTIAL, UNIFORM, TRIANGULAR,
       WEIBULL
 Case "BETADIST":  a1 = para(1):  a2 = para(2):  a3 = para(3):  a4 = para(4)
                   x_i = .BetaInv(.NormSDist(ni), a1, a2, a3, a4)
 Case "GAMMA":    alpha = para(1): lambda = para(2)
                   x_i = .GammaInv(.NormSDist(ni), alpha, lambda)
 Case "PERTDIST":   a1 = para(1):  a2 = para(2):  a3 = para(3)
          lambda1 = 4 * (a2 - a1) / (a3 - a1) + 1: lambda2 = 4 * (a3 - a2) / (a3 - a1) + 1
          x_i = .BetaInv(.NormSDist(ni), lambda1, lambda2, a1, a3)
End Select
End With
End Function
```

Each case one or two lines only

As in Low and Tang (2007)

More succinct than the 24 lines in Low and Tang (2007)

Transforming n_i to original random variables x_i for use in performance function g(**x**)

Fig. 10 Tranforming FORM template to MCS by adding a random u column

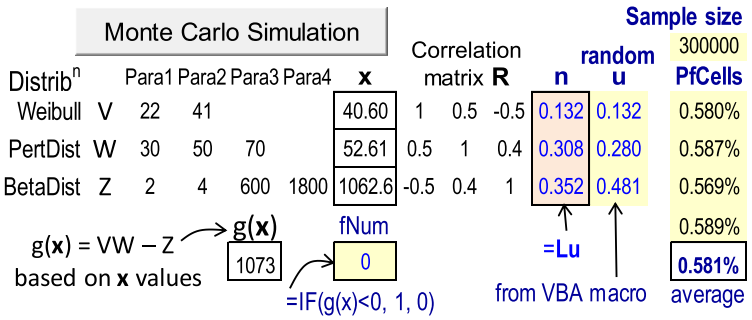


```
Sub MonteCarloSimulation()
'Define cell names for SampleSize, fNum, random_u, and PfCells (1 or several),
Dim TempVector() As Double
ntrial = 300000:  StartTime = Timer:  Range("SampleSize").Value = ntrial
n = Range("random_u").Count:  ReDim TempVector(1 To n)
Range("PfCells").ClearContents: Range("random_u").ClearContents
Application.ScreenUpdating = False
For k = 1 To Range("PfCells").Count
Sum = 0
Randomize (Timer)
For i = 1 To ntrial
 For j = 1 To n
  Number = Rnd():  If Number <= 10 ^ (-15) Then Number = 10 ^ (-15)
  If Number >= 1 - 10 ^ (-15) Then Number = 1 - 10 ^ (-15)
  TempVector(j) = WorksheetFunction.NormSInv(Number)
 Next j
 Range("random_u").Value = WorksheetFunction.Transpose(TempVector)
 Sum = Sum + Range("fNum").Value
 ProbFail = WorksheetFunction.RoundDown(Sum / i, 6) * 100
 Application.StatusBar = i & " trials completed, " & Sum & " failures, " & "Pf = " & ProbFail & "%"
Next i
Range("PfCells").Cells(k).Value = Sum / ntrial
Next k
MsgBox (Timer - StartTime) & " seconds"
Application.ScreenUpdating = True
End Sub
```

Monte Carlo simulation in Excel for correlated nonnormal distributions

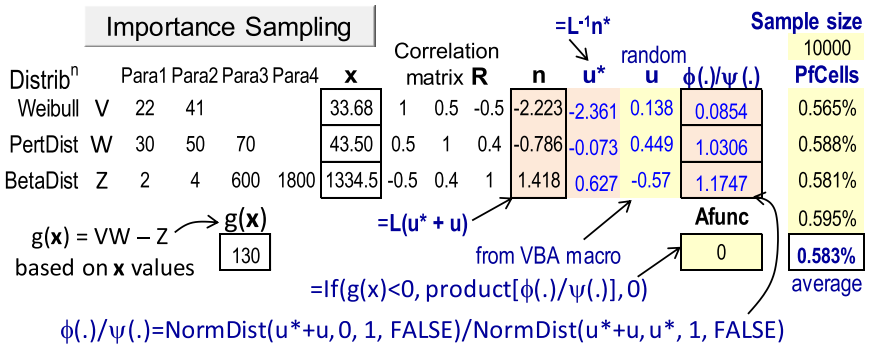

in which $\mathbf{u}^* = \mathbf{L}^{-1}\mathbf{n}^*$, where $\mathbf{L}^{-1}$ is the inverse of the Cholesky lower decomposed matrix of **R**, and **n*** is the FORM solution of **n*** values in Fig. 1

```
Sub ImportanceSampling ()
'Define cell names for Afunc, SampleSize, random_u, PfCells (1 or a few)
Dim TempVector() As Double
ntrial = 10000:   StartTime = Timer:   Range("SampleSize").Value = ntrial
Range("PfCells").ClearContents:  Range("random_u").ClearContents
n = Range("random_u").Count:   ReDim TempVector(1 To n)
Application.ScreenUpdating = False
For k = 1 To Range("PfCells").Count
Sum = 0:   Randomize (Timer)
For i = 1 To ntrial
 For j = 1 To n
   Number = Rnd():    If Number <= 10 ^ (-15) Then Number = 10 ^ (-15):
   If Number >= 1 - 10 ^ (-15) Then Number = 1 - 10 ^ (-15)
   TempVector(j) = WorksheetFunction.NormSInv(Number)
 Next j
 Range("random_u").Value = WorksheetFunction.Transpose(TempVector)
 Sum = Sum + Range("Afunc").Value:   ProbFail = WorksheetFunction.RoundDown(Sum / i, 6)
 Application.StatusBar = i & " trials completed, Pf = " & ProbFail * 100 & "%"
Next i
Range("PfCells").Cells(k).Value = Sum / ntrial
Next k
MsgBox (Timer - StartTime) & " seconds":   Application.ScreenUpdating = True
End Sub
```

Importance Sampling in Excel, Ref. Melchers (1984), Chan (2012, Appendix C)

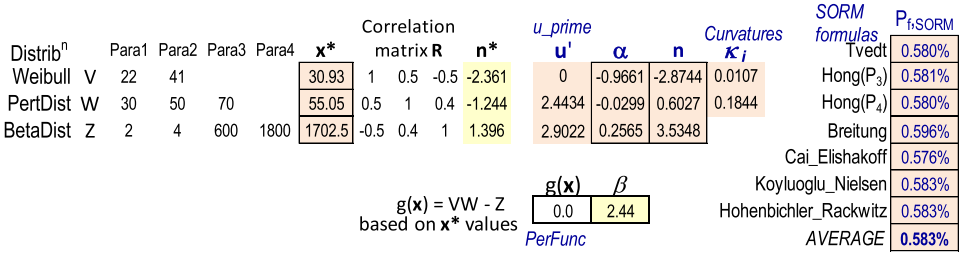

- Runs a VBA sub-procedure (macro) **CurvaturesKappa()** to compute curvatures κ_i.
- The number of curvatures (κ_i) is equal to the number of random variables minus one.
- The column labelled $\alpha = (\mathbf{L}^{-1}\mathbf{n}^*)/\beta$ = mmult(minverse(cholesky(CrMatrix)),**n***)/β
- The column labelled **n** = mmult(cholesky(CrMatrix),mmult(minverse(GramSchmidt(α)),u_prime))

SORM, after Chan and Low (2012), https://doi.org/10.1002/nag.1057

Funding 'Open Access funding provided by the MIT Libraries'.

Declarations

Conflict of interest The authors have no relevant financial or non-financial interests to disclose.

Open Access This article is licensed under a Creative Commons Attribution 4.0 International License, which permits use, sharing, adaptation, distribution and reproduction in any medium or format, as long as you give appropriate credit to the original author(s) and the source, provide a link to the Creative Commons licence, and indicate if changes were made. The images or other third party material in this article are included in the article's Creative Commons licence, unless indicated otherwise in a credit line to the material. If material is not included in the article's Creative Commons licence and your intended use is not permitted by statutory regulation or exceeds the permitted use, you will need to obtain permission directly from the copyright holder. To view a copy of this licence, visit http://creativecommons.org/licenses/by/4.0/.

References

Ang HS, Tang WH (1984) Probability Concepts in Engineering Planning and Design, Vol. II: Decision, Risk, and Reliability, John Wiley and Sons, New York, 562 pp.

Baecher GB, Christian JT (2003) Reliability and Statistics in Geotechnical Engineering. John Wiley, Chichester, West Sussex, England; Hoboken, NJ.

Boon CW, Houlsby GT, Utili S (2015a) Designing tunnel support in jointed rock masses Via the DEM. Rock Mech Rock Eng 48:603–632

Boon CW, Ooi LH, Low YY, (2015b) Performance of ground anchors in a Mass Rapid Transit project in Malaysia. Field Monitoring in Geomechanics (FMGM), PM. Dight (Ed.), Australian Centre for Geomechanics, pp. 621–630.

Boon CW, Ooi LH, Tan JG, Goh CY (2019) Deep excavation of an underground metro station in karstic limestone: a case history in the Klang Valley SSP Line. Proceedings in Geotechnics for Sustainable Development, GEOTEC HANOI, D.L. Phung, T.D. Nguyen (Eds.), pp 423–430.

Chan CL, Low BK (2012) Practical second-order reliability analysis applied to foundation engineering. International J. for Numerical and Analytical Methods in Geomechanics, Wiley, 36 (11), 1387–1409.

Chan CL (2012) Reliability assessment of laterally loaded single piles. Doctoral thesis, Nanyang Technological University, Singapore. https://dr.ntu.edu.sg/bitstream/10356/48201/1/TCG0603380K.pdf

Dadashzadeh N, Duzgun HSB (2017) Reliability-based stability analysis of rock slopes using numerical analysis and response surface method. Rock Mech Rock Eng 50:2119–2133. https://doi.org/10.1007/s00603-017-1206-2

Der Kiureghian A, Liu PL (1986) Structural reliability under incomplete probability information. Journal of Engineering Mechanics, ASCE 112(1):85–104

Ditlevsen O (1981) Uncertainty Modeling: With Applications to Multidimensional Civil Engineering Systems. McGraw-Hill, New York

Goodman RE (1995) Thirty-fifth Rankine lecture: 'Block theory and its application.' Geotechnique 45(3):383–423

Goodman RE, Taylor RL, (1967) Methods of analysis for rock slopes and abutments: A review of recent developments, Failure and Breakage of Rocks, edited by C. Fairhurst, AIME, pp. 303–320.

Haldar A, Mahadevan S (2000) Probability, Reliability, and Statistical Methods in Engineering Design. John Wiley and Sons Inc, New York

Hasofer AM, Lind NC (1974) Exact and invariant second-moment code format. J Eng Mechanics, ASCE 100:111–121

Hencher SR, Lee SG, Carter TG, Richards LR (2011) Sheeting joints: characterisation, shear strength and engineering. Rock Mech Rock Eng 44:1–22. https://doi.org/10.1007/s00603-010-0100-y

Hendron AJ, Cording, EJ, and Aiyer, AK (1971) Analytical and graphical methods for the analysis of slopes in rock masses, U.S. Army Engrg. Nuclear Cratering Group Technical Rep. No. 36

Hoek E, Bray JW, Boyd JM (1973) The stability of a rock slope containing a wedge resting on two intersecting discontinuities. Q J Eng GeolHydrogeol 6(1):1–55

Hoek E, Bray JW (1981) Rock Slope Engineering, Revised 3rd edition, The Institution of Mining and Metallurgy, London, 1981, pp 337 - 351.

Hoek E (2023) Practical rock engineering. https://www.rocscience.com/learning/hoeks-corner

Jaeger JC (1971) Friction of rocks and the stability of rock slopes. Geotechnique 21(2):97–134

Jimenez-Rodriguez R (2007) Rock wedge stability analysis using system reliability methods. Rock Mech Rock Engng 40:419–427. https://doi.org/10.1007/s00603-005-0088-x

John KW (1968) Graphical stability analysis of slopes in jointed rock. J Soil Mechan Foundations Division, ASCE 94(2):497–526

Kottegoda NT, Rosso R (2008) Applied Statistics for Civil and Environmental Engineers, 2nd edn. Wiley-Blackwell, New York, p 736

Kumsar H, Aydan Ö, Ulusay R (2000) Dynamic and static stability assessment of rock slopes against wedge failures. Rock Mechan Rock Eng 33:31–51

Londe P, Vigier G, Vormeringer R (1969) The stability of rock slopes, a three-dimensional study. J Soil Mech Foundations Division, ASCE 95(1):235–262

Low BK (1997) Reliability analysis of rock wedges. J Geotech Geoenviron Eng 123(6):498–505

Low BK (2020) Correlated sensitivities in reliability analysis and probabilistic Burland-and-Burbidge method. Georisk Assessment Manag Risk Fengineered Syst Geohazards 16(3):397–412. https://doi.org/10.1080/17499518.2020.1861636

Low BK (2022) Context-dependent parameter sensitivities in rock slope stability. Rock Mech Rock Eng 55:7445–7468. https://doi.org/10.1007/s00603-022-03017-0

Low BK, Bathurst RJ (2022) Load-resistance duality and case-specific sensitivity in reliability-based design. Acta Geotech 17:3067–3085

Low BK, Einstein HH (2013) Reliability analysis of roof wedges and rockbolt forces in tunnels. Tunn Undergr Space Technol 38:1–10. https://doi.org/10.1016/j.tust.2013.04.006

Low BK, Tang WH (2004) Reliability analysis using object-oriented constrained optimization. Struct Saf 26(1):69–89

Low BK, Tang WH (2007) Efficient spreadsheet algorithm for first-order reliability method. J Eng Mech. https://doi.org/10.1061/(ASCE)0733-9399(2007)133:12(1378)

Low BK, Zhang J, Tang WH (2011) Efficient system reliability analysis illustrated for a retaining wall and a soil slope. Computers and Geotechnics, Elsevier 38(2):196–204

Low BK, (2021) Reliability-based design in soil and rock engineering: enhancing partial factor design approaches. CRC Press, 399 pages. https://www.routledge.com/9780367631390

Macciotta R, Martin CD, Morgenstern NR et al (2016) Quantitative risk assessment of slope hazards along a section of railway in the Canadian Cordillera—a methodology considering the uncertainty in the results. Landslides 13:115–127. https://doi.org/10.1007/s10346-014-0551-4

Madsen HO, Krenk S, Lind NC (1986) Methods of Structural Safety. Prentice Hall, NJ, p 403

Melchers RE (1987) Structural Reliability: Analysis and Prediction. Ellis Horwood Ltd., Chichester, West Sussex, England

Melchers RE, Beck AT (2018) Structural Reliability: Analysis and Prediction, 3rd edn. John Wiley, New York

Melchers RE, (1984) Efficient Monte-Carlo probability integration. Research Report No. 7, Department of Civil Engineering, Monash University, Clayton, Australia.

Park H, West TR (2001) Development of a probabilistic approach for rock wedge failure. Eng Geol 59(3–4):233–251. https://doi.org/10.1016/S0013-7952(00)00076-4

Priest SD (1993) Discontinuity analysis for rock engineering. Chapman and Hall, London

Rackwitz R (2001) Reliability analysis: A review and some perspectives. Structural Safety, Elsevier 23(4):365–395

Rackwitz R, Fiessler B (1978) Structural reliability under combined random load sequences. Computers & Structures, Elsevier 9:484–494

Rocscience Inc (2002). SWedge Probabilistic analysis of the geometry and stability of surface wedges

User's Guide Rocscience Inc (2022) SWedge verification manual. https://www.rocscience.com/help/swedge/verification-theory/verification-manuals

Shinozuka M (1983) Basic analysis of structural safety. J Struct Engrg ASCE 109(3):721–740

Simpson B, Vogt N, van Seters AJ (2011) Geotechnical safety in relation to water pressures. ISGSR 2011 - Vogt, Schuppener, Straub & Bräu (eds) - © 2011 Bundesanstalt für Wasserbau ISBN 978–3–939230–01–4, p501–517

Simpson B, (2007) Approaches to ULS design–The merits of Design Approach 1 in Eurocode 7. ISGSR2007 First International Symposium on Geotechnical Safety and Risk, Shanghai. Tongji University, China

Tichy M (1993) Applied Methods of Structural Reliability. Kluwer Academic, Dordrecht, Boston

Wang YJ, Yin JH, Chen Z, Lee CF (2004) Analysis of wedge stability using different methods. Rock Mech and Rock Engrg 37:127–150. https://doi.org/10.1007/s00603-003-0023-y

Wittke W (1990) Rock mechanics: theory and applications with case histories (English translation). Springer-Verlag, New York

Wyllie DC, (1999) Foundations on rock, 2nd ed., 435 pages, E & FN Spon, London.

Wyllie DC, (2018) Rock Slope Engineering, Civil Applications, 5th Ed., Based on the third edition by Evert Hoek and John Bray, CRC Press, Taylor and Francis Group, Boca Raton.

Publisher's Note Springer Nature remains neutral with regard to jurisdictional claims in published maps and institutional affiliations.